agronomy

MDPI

Review

Visualization Techniques for Spray Monitoring in Unmanned Aerial Spraying Systems: A Review

Jungang Ma [1,2], Hua Zhuo [1,2], Peng Wang [1,2], Pengchao Chen [3], Xiang Li [3], Mei Tao [1,2] and Zongyin Cui [3,*]

[1] Xinjiang Agricultural Unmanned Aircraft Performance and Safety Key Laboratory, Urumqi 830011, China
[2] Xinjiang Uygur Autonomous Region Research Institute of Measurement and Testing, Urumqi 830011, China
[3] National Center for International Collaboration Research on Precision Agricultural Aviation Pesticides Spraying Technology (NPAAC), South China Agricultural University, Guangzhou 510642, China
* Correspondence: zcui@stu.scau.edu.cn

Abstract

Unmanned Aerial Spraying Systems (UASS) has rapidly advanced precision crop protection. However, the spray performance of UASSs is influenced by nozzle atomization, rotor-induced airflow, and external environmental conditions. These factors cause strong spatiotemporal coupling and high uncertainty. As a result, visualization-based monitoring techniques are now essential for understanding these dynamics and supporting spray modeling and drift-mitigation design. This review highlights developments in spray visualization technologies along the "droplet–airflow–target" chain mechanism in UASS spraying. We first outline the physical fundamentals of droplet formation, liquid-sheet breakup, droplet size distribution, and transport mechanisms in rotor-induced flow. Dominant processes are identified across near-field, mid-field, and far-field scales. Next, we summarize major visualization methods. These include optical imaging (PDPA/PDIA, HSI, DIH), laser-based scattering and ranging (LD, LiDAR), and flow-field visualization (PIV). We compare their spatial resolution, measurement range, 3D reconstruction capabilities, and possible sources of error. We then review wind-tunnel trials, field experiments, and point-cloud reconstruction studies. These studies show how downwash flow and tip vortices affect plume structure, canopy disturbance, and deposition patterns. Finally, we discuss emerging intelligent analysis for large-scale monitoring—such as image-based droplet recognition, multimodal data fusion, and data-driven modeling. We outline future directions, including unified feature systems, vortex-coupled models, and embedded closed-loop spray control. This review is a comprehensive reference for advancing UASS analysis, drift assessment, spray optimization, and smart support systems.

Keywords: unmanned aerial spraying system; spray visualization; droplet transport; rotor-induced airflow; multimodal fusion; intelligent analysis

Check for updates

Academic Editor: Jayme Garcia Arnal Barbedo

Received: 26 November 2025
Revised: 17 December 2025
Accepted: 22 December 2025
Published: 4 January 2026

Copyright: © 2026 by the authors. Licensee MDPI, Basel, Switzerland. This article is an open access article distributed under the terms and conditions of the Creative Commons Attribution (CC BY) license.

1. Introduction

The global adoption of Unmanned Aerial Spraying Systems (UASSs) is advancing rapidly; however, implementation is constrained by varying degrees of regulation across regions. In the European Union, aerial pesticide spraying is strictly regulated, with exceptions permitted in only 5% of cases following a risk assessment [1,2]. In North America, regulations are relatively lenient, with a licensing system that requires both aviation qualifications and dual certification for pesticide application [3]. In South America, Brazil requires multi-departmental coordination and flight licensing, whereas Argentina has simplified

the approval process for small drones [4]. In Asia, drone spraying technology is spreading rapidly, though regulatory frameworks are not yet standardized. Countries such as China, Korea, and Japan have begun establishing registration and certification systems, whereas other nations are still refining their regulations [2,5,6]. Australia places particular emphasis on aircraft safety and environmental protection, requiring strict adherence to operational standards for pesticide spraying [5,7]. Despite significant differences in regulations governing the global use of drones for pesticide spraying, spray monitoring technologies remain critical for assessing operational effectiveness, reducing drift risks, and ensuring safe application [8]. Using visualization technologies, it is possible to capture spray trajectories, droplet dynamics (including motion, breakup, and transport), and deposition patterns in real time, thereby optimizing operational parameters and ensuring the accuracy and safety of spraying processes under various environmental conditions.

With the rapid adoption of unmanned aerial spraying systems (UASSs) in crop protection, these platforms have demonstrated notable advantages in precise pesticide application, improved operational efficiency, and adaptability to complex terrains such as hilly regions and orchards [9–11]. However, droplets generated during UASS spraying must travel over relatively long distances, and their trajectories exhibit pronounced transience and uncertainty under the combined influence of rotor-induced flow, ambient meteorological conditions, and crop canopy structure [11,12]. After leaving the nozzle, droplets undergo a series of multiscale, multiphysical processes, including liquid-film rupture, droplet formation, turbulent transport, evaporation, and deposition. These processes lead to significant variations in spray performance, including application uniformity, droplet utilization, and drift safety, across different operational conditions. While international standards for the technical assessment of UASS spray performance exist, they are still not fully developed. For example, ISO 16122-5:2020 [13], ISO 5682-1:2017 [14], and ISO 24253-1:2015 [15] primarily focus on the spray deposition effects of crop protection equipment and employ traditional measurement methods, such as water-sensitive papers, for droplet collection. However, these standards do not address visualization technologies and related standards specifically for the quality of drone-based spraying. In addition, Variable Rate Technology (VRT), a key innovation in precision agriculture, enables site-specific application of inputs such as pesticides and fertilizers through the integration of GPS, sensors, and prescription maps, and has become a significant area of development in precision spraying [16]. In the future, spray visualization techniques are expected to serve as core diagnostic tools for evaluating VRT performance and optimizing spray quality, providing essential technical support for intelligent and adaptive control of UASS-based spraying systems. Therefore, a thorough understanding of droplet transport mechanisms, driven by flow-field interactions, and disturbance behaviors in the UASS spraying process is of great theoretical and engineering significance for optimizing nozzle design, improving flight operational parameters, reducing drift risks, advancing VRT technologies, and informing the development of related standards. Therefore, a comprehensive understanding of droplet transport mechanisms and disturbance behaviors during the UASS spraying process is of significant theoretical and engineering importance for optimizing nozzle design and flight operational parameters, thereby reducing drift risks, advancing VRT technologies, and supporting the development of relevant standards.

The spatial distribution, size spectrum, and dynamics of droplets are determined by nozzle atomization, liquid sheet breakup, rotor downwash, and environmental conditions [11,17]. Conventional drift assessment methods (e.g., water-sensitive paper, collection plates, filter papers) provide partial deposition information but are subject to inherent limitations. In particular, water-sensitive paper measurements are affected by card orientation and saturation under high deposition conditions, while sampling de-

vices may introduce flow disturbance and associated biases. More fundamentally, these methods lack the temporal and spatial resolution required to capture in-flight droplet transport and the three-dimensional, transient evolution of spray plumes and rotor–spray interactions, thereby limiting their suitability for mechanistic analysis and parameter optimization [11,18]. Optical and laser-based visualization techniques—such as PDIA (Particle/Droplet Image Analysis), HSI (high-speed imaging), high-speed shadowgraphy, digital inline holography (DIH), laser imaging, PDPA (Phase Doppler Particle Analysis), and LiDAR—are now core tools in agricultural spray research [11,19,20], initially focused on nozzle atomization evaluation. Under UASS conditions, rotor downwash increases aerodynamic loads, widens the spray, and complicates droplet fields. Thus, measurement methods must meet new demands regarding spatial coverage, temporal resolution, and data fusion. Spatial coverage is particularly critical for accurate atomization analysis, as it directly influences the uniformity and precision of spray deposition. These factors raise the performance requirements for spray visualization techniques [9,11].

UASS spray characteristics depend on both droplet properties and rotor-induced flow effects. From a physical perspective, rotor-induced airflow can be broadly categorized into primary downwash, rotor-tip vortices, and ground-effect–modulated flow, each playing distinct roles in droplet transport. The primary downwash dominates near-ground transport and deposition patterns, whereas rotor-tip vortices may induce uplift and secondary transport, contributing to low-intensity long-range drift [11,21]. In addition, ground effects can significantly alter near-surface flow structures and droplet redistribution. In complex environments such as fruit tree canopies, rotor-induced airflow interacts with canopy structures to generate multiscale turbulence. Rotor downwash and associated vortices dominate macro-scale canopy disturbance, while leaf- and branch-level motion produces micro-scale turbulence that influences droplet interception, penetration, and redistribution [11,22]. Thus, droplet visualization and flow-field visualization together enable a complete understanding of UASS spray performance through their complementary perspectives—one explains transport and deposition, the other reveals flow structure and droplet–flow coupling. Integration of both establishes a thorough mechanistic foundation for precision application modeling [11,23].

Recent advances in three-dimensional sensing and multimodal imaging have enabled non-contact, real-time monitoring of agricultural sprays. Zhang et al. [11,24] demonstrated that LiDAR retrieves spray cloud volume, centerline trajectory, and drift distance (with errors <7%), infrared thermography infers deposition patterns from temperature variations, and spectroscopic methods identify chemical composition and predict drift. Chegini et al. [11,25] highlighted that LiDAR backscatter, leaf wetness sensors (LWS), and DIH are complementary: LiDAR reconstructs far-field structure, DIH measures droplet sizes from 20 μm to millimeters, and LWS monitors deposition quality online. These methods are applicable across a wide range of crops, particularly in complex agricultural environments. Regarding measurement intrusiveness, Molnar-Irimie et al. [11,26] classified techniques as intrusive or non-contact and noted that non-contact optical methods are poised to become the mainstream in spray dynamics research.

This review offers a thorough analysis of global research on spray visualization techniques, with a primary focus on studies published 2000 and 2025. Approximately 80% of the studies examined were sourced from the Web of Science Core Collection (WOSCC), all of which are accessible through Google Scholar. By exploring key terms, research trends, and technological advancements, this review highlights significant development trends and emerging frontiers in the field.

Building on existing deposition-based assessments, and in contrast to prior reviews that primarily focus on deposition outcomes, drift metrics, or individual sensing tech-

niques, this review systematically integrates spray visualization with droplet–flow coupling analysis to provide a unified perspective on UASS spray transport. It is organized around a coherent framework linking droplet atomization, rotor-induced flow and plume evolution, canopy interaction, and data-driven modeling. Advances in droplet–flow coupling, canopy disturbance, and 3D drift monitoring are addressed.

In addition to summarizing the current state of research, this review introduces sev-eral novel contributions. First, it emphasizes multiscale mapping methods, linking them directly to physical variables, which enhances our understanding of spray dynamics across different spatial scales. Second, the review highlights the significant role of multimodal techniques in improving the accuracy and reliability of spray monitoring. By integrating various visualization technologies such as LiDAR, DIH, and LWS, this approach fosters standardization and facilitates the development of reliable indicators for UASS ap-plications. Lastly, we define deployability criteria across lab, wind tunnel, and field envi-ronments, providing insight into the specific standards and applicability of these tech-niques, and helping readers understand the limitations and ideal use cases for each. Particular attention is given to current methodological limitations and scalability challenges, and future research directions are discussed to support UASS precision application and droplet transport model development.

2. Physical Basis of Droplet and Rotor-Induced Flow Field

The droplet–airflow system formed during UASS spraying operations represents a typical multiphase flow coupling process, as shown in Figure 1. From ejection at the nozzle to deposition on the target, droplets undergo successive stages of atomization, transport, dispersion, and redistribution, while the rotor-induced flow field provides the dominant energy input and disturbance environment throughout this process [11,27]. This chapter centers on this core process and elaborates the physical basis of UASS spraying from three perspectives: (1) droplet formation and initial characteristics; (2) droplet motion, referring to the movement and trajectory of droplets within the rotor flow; and (3) the coupling relationship between droplets and the flow field, as well as the associated visualization requirements.

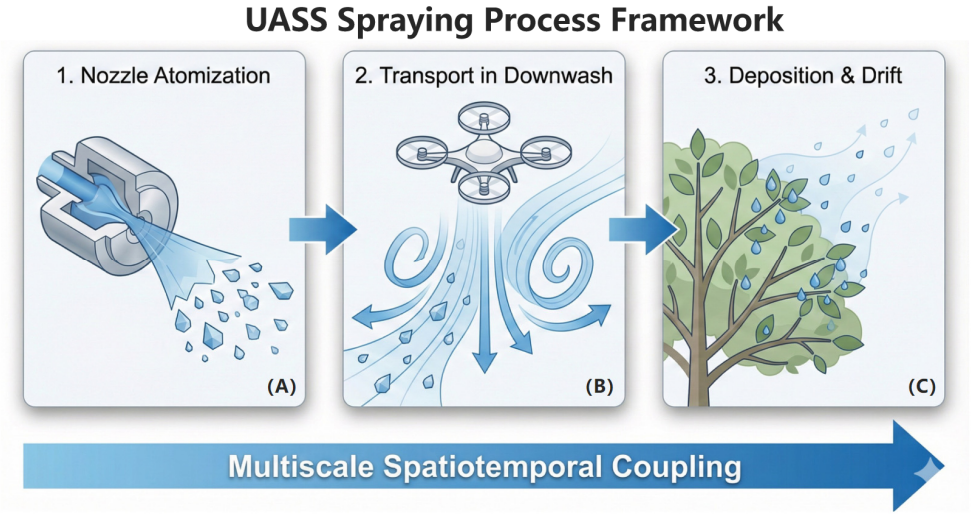


Figure 1. Multiscale spatiotemporal coupling in the UASS spraying process. Note: The arrows between (**A**–**C**) show the sequential progression of the spray process. The arrow in (**B**) indicates downwash airflow, and the arrow in (**C**) represents droplet drift, showing droplets escaping the target. The figure concept was assisted by the Gemini 3.0 AI model developed by Google LLC (Mountain View, CA, USA); the final illustration was manually produced using Microsoft PowerPoint (Microsoft Corporation, Redmond, WA, USA).

2.1. Droplet Formation and Initial Characteristics

2.1.1. Nozzle Types and Initial Droplet Generation Mechanisms

The initial stage of UASS spraying is determined by the nozzle's structure and operating principle. Common nozzles can be broadly classified into hydraulic nozzles and centrifugal nozzles. In the Americas and Asia, research on droplet dynamics has primarily focused on the control of spray pressure and droplet size. Hydraulic nozzles rely on liquid pressure to force the spray solution through the orifice and form a liquid sheet, which breaks up into droplets under the combined action of aerodynamic forces and surface tension. An increase in spray pressure effectively raises the Reynolds and Weber numbers, which are key parameters in the atomization/regime transition [9]. The Reynolds number characterizes the flow regime and determines the dominance of inertial or viscous forces. In contrast, the Weber number indicates the relative importance of aerodynamic forces versus surface tension in the breakup process. At low Weber numbers, Rayleigh–Plateau breakup prevails, whereas at high Weber numbers, aerodynamic breakup becomes dominant. This leads to thinner liquid sheets, enhanced breakup, and consequently smaller droplets with higher initial velocities; however, such fine droplets are more susceptible to air disturbances and therefore more prone to drift [11,24]. Air-induction nozzle (AIN) is an improved form of hydraulic nozzles that introduce air bubbles into the liquid stream, producing low-density, larger air-filled droplets and thereby reducing drift risk. Such nozzles have been widely applied in ground boom spraying and in some low-altitude UASS operations [28]. In recent years, centrifugal nozzles have developed rapidly in the UASS domain. Their core component is a high-speed rotating disc or cup: the spray liquid flows radially along the disc surface under centrifugal force, forming a thin liquid film at the rim, which then breaks up into fine droplets. The droplet size can be continuously controlled by adjusting the rotational speed, as changes in rotational speed modify the liquid film thickness and flow velocity, thereby altering the Reynolds and Weber numbers that govern film instability and droplet-size distribution [29]. Compared with hydraulic nozzles, centrifugal nozzles offer advantages such as low operating pressure, adjustable droplet spectrum, and compatibility with multiple formulation types. They are particularly suitable for integration with PWM control and electronic speed regulation, enabling the construction of variable-speed spraying systems for multirotor UASSs [30].

In European studies, greater emphasis has been placed on the relationship between nozzle geometry and the initial droplet formation process. Tadić et al. [31] reported that hydraulic nozzles remain dominant in European orchard operations, but nozzle orifice design prioritizes liquid-film thickness and atomization uniformity over increased spray pressure. In contrast to research in the Americas and Asia, which tends to target finer droplets to enhance canopy penetration, European studies emphasize balancing low drift with high deposition efficiency by optimizing liquid-film breakup and air-induction processes. Similar perspectives have been reported by Cerruto et al. [32] and Nogueira et al. [33], who argued that controlling liquid film stability is more effective for improving spray consistency than simply increasing spray pressure.

International studies on initial droplet characteristics further indicate that nozzle type determines not only droplet size but also key variables, including initial velocity, spray angle, and droplet number density. Wind-tunnel measurements by Dorr et al. [34] showed that nozzle structure has a much stronger influence than spray formulation on $Dv_{0.5}$, initial velocity, spray angle, and liquid distribution density. Droplets exhibit nearly uniform initial velocities in the region near the nozzle outlet (0–50 mm), while differences in droplet size mainly emerge in the far-field aerodynamic process, underscoring the dominant role of nozzle geometry in setting the initial dynamical conditions. The study also pointed out that AIN, due to air entrainment in the internal cavity, can substantially reduce effective

liquid density (down to 701–1000 kg/m^3), thereby generating larger, low-density droplets that increase deposition probability and reduce drift sensitivity. With regard to nozzle selection and configuration for agricultural UASSs, Yu et al. [35] systematically tested 18 commonly used UASS nozzles and found that the actual flow rates generally agreed with the manufacturer's nominal values (within ±3.5%), whereas spray angle deviations could reach 10%, which has a significant impact on swath overlap and application uniformity. In addition, the measured droplet spectra from various XR (hydraulic flat fan nozzles), TP (hydraulic cone nozzles), and TX (hydraulic twin-nozzle nozzles) series nozzles were consistently finer than their nominal classifications. With increasing pressure, the spray angle increased approximately linearly while the liquid film thickness decreased, further reducing droplet size [36]. Taken together, these results demonstrate that nozzle type, geometric structure, and actual operating pressure jointly determine the initial, near-field droplet spectrum and spray pattern in UASS spraying, providing a basis for UASS design and parameter optimization.

2.1.2. Dynamics of Liquid Sheet Breakup and Mechanisms of Drop Size Distribution Formation

Droplet formation in agricultural nozzles is governed by the breakup dynamics of the liquid sheet and can be broadly categorized into two typical mechanisms. The first is the surface-tension-dominated Rayleigh–Plateau instability, in which disturbances on the liquid sheet grow, leading to the formation and rupture of ligaments and liquid bridges, producing relatively large droplets [37]. The second is aerodynamic sheet breakup, driven by aerodynamic forces, in which the liquid sheet is torn apart by high-velocity jets or strong aerodynamic shear, resulting in a finer droplet distribution [29]. The dominant breakup regime is generally determined by the Weber number: at low Weber numbers, the Rayleigh–Plateau mode prevails, whereas at high Weber numbers, aerodynamic breakup becomes dominant.

Canu et al. [37] further noted that liquid sheet breakup typically proceeds through several stages, including sheet formation, disturbance growth, ligament generation, and droplet pinch-off. The sheet thickness and disturbance wavelength together determine the final drop size distribution, and bimodal spectra often reflect the superposition of sheet rupture and ligament breakup mechanisms [28]. The internal geometry of the nozzle sets the initial sheet thickness and velocity distribution, which are key initial conditions that control the subsequent disturbance growth rate and breakup mode [38]. For UASSs, rotor downwash substantially intensifies local aerodynamic loading within the spray swath, which more readily triggers aerodynamic breakup, shifting the drop-size distribution toward medium and small droplets and broadening the overall size range.

By combining liquid sheet disturbance models with HSI, atomization in agricultural nozzles can be understood as a unified process: primary disturbances cause local thinning of the liquid sheet and the formation of holes; these holes expand under aerodynamic forces and collide to form liquid bridges; the bridges then undergo Rayleigh–Plateau instability and break up into final secondary droplets [37,39]. They specifically highlighted that hole opening angle and liquid bridge area are strongly correlated with the fraction of fine droplets, providing direct evidence for a hole-driven breakup mechanism in agricultural spraying.

2.1.3. Initial Droplet Velocity, Velocity Fluctuations, and Standardized Measurement Framework

Accurate measurement of the droplet size distribution is a prerequisite for understanding the atomization process and constructing spray models. The diversity of droplet-sizing techniques across studies has led to limited comparability of results. According to international standards such as ISO 25358:2018 [40], inter-experimental calibration and alignment

of results should be achieved using BCPC (British Crop Protection Council) reference nozzles or equivalent cumulative-size distribution curves. This standardized framework not only facilitates consistent evaluation of droplet spectra across different nozzle types and pressure conditions, but also provides reliable, comparable boundary conditions for spray–flow coupling models. Nevertheless, these standards are primarily developed for ground-based, quasi-steady spraying systems, and their direct application to UASS remains limited for several reasons. First, UASS spraying involves three-dimensional transient flow induced by rotor downwash, which differs from the steady-state conditions for which these standards were developed. Second, the rotor-spray-canopy coupling in UASS creates complex interactions that significantly affect spray performance, which traditional ground-based models cannot fully account for. Third, measurement variability due to dynamic UASS conditions makes consistent application of standardized methods challenging, as spray patterns can vary with flight height and operational conditions. In this context, spray visualization techniques play a critical role by enabling in situ characterization of droplet–flow dynamics and providing complementary information beyond standardized droplet-size metrics.

Centrifugal nozzles, which currently dominate the UASS market, still lack effective methods for measuring droplet size. This limitation is largely attributed to the instability of liquid film breakup and the strong coupling between rotational speed and atomization behavior, making them fundamentally different from hydraulic nozzles in terms of droplet characterization [41]. Unlike the quasi-two-dimensional fan-shaped structure produced by hydraulic nozzles, sprays from centrifugal nozzles exhibit pronounced three-dimensional dispersion characteristics, with significant gradients in droplet size distribution both radially and axially. Consequently, traditional sizing methods based on a single measurement plane or fixed traverse paths are difficult to apply effectively. Additionally, droplet sizing is highly sensitive to spray flow rate; even small changes in flow rate can significantly alter the structure of the droplet size distribution. These factors contribute to the inherent uncertainties in droplet sizing for centrifugal nozzles, which are further compounded by the measurement position, flow rate, and the complex three-dimensional nature of the spray field [42].

In addition to droplet size, the initial droplet velocity and its fluctuation characteristics are crucial links connecting atomization processes with drift behavior. Wang et al. [43] conducted a systematic analysis using PIV (particle image velocimetry) to examine the atomization characteristics, velocity distribution, and velocity fluctuations of three typical nozzles: IDK (air-induction flat fan), ST (standard flat fan), and TR (hollow-cone swirl). The study, in combination with Helos laser diffraction and wind-tunnel deposition tests, examined the impact of nozzle configuration on droplet dynamics and drift risk. Results indicated that IDK nozzles produced larger droplets with lower velocities and less fluctuation, resulting in reduced drift. In contrast, ST nozzles generated smaller droplets with higher velocity fluctuations. The velocity fluctuations, which were most pronounced in the ST nozzle (4.54 m/s), played a key role in controlling drift, particularly for small droplets ($V < 75$ and $V < 100$). These findings underscore the importance of nozzle type, geometric structure, and pressure settings in shaping the spray characteristics and drift behavior of UASS, providing valuable insights for optimizing drone spraying systems.

In summary, nozzle geometry, operating pressure, and liquid sheet breakup mechanisms collectively determine the initial conditions of UASS spraying—including droplet size, velocity, and spectral width. These "initial boundary conditions" shape subsequent transport, deposition, and drift behavior by governing how droplets respond to the rotor-induced flow field.

2.2. Droplet Motion and Evolution in Rotor Flow

2.2.1. Fundamental Mechanisms of Rotor-Induced Flow on Droplet Transport

Immediately after leaving the nozzle, droplets are subjected to the rotor-induced flow field, as shown in Figure 1. The high-speed rotation of multirotor blades generates a characteristic downwash flow, producing tip vortices and recirculation structures with strong shear in the blade tips. Related studies have shown that these vortical structures significantly alter the original spray distribution, distorting and displacing droplet trajectories [44]. Once the spray enters the downwash region, droplet motion is jointly governed by droplet inertia and aerodynamic drag. From a physical standpoint, droplet–flow coupling can be described by the Stokes number (St), defined as the ratio of the droplet response time to the characteristic flow timescale. Droplets with higher St are more inertia-dominated and can penetrate vortical structures and deposit rapidly, whereas droplets with low St tend to follow turbulent motions, leading to prolonged residence in wakes, recirculation zones, or upward entrainment for redistribution [45].

Rotor speed, UASS flight height, and forward speed collectively influence the intensity of downwash and the morphology of rotor-induced vortices. Under hovering or low-speed conditions, the downwash typically exhibits a near-axisymmetric structure. As forward speed increases, the downwash jet is progressively deflected downstream, resulting in a backward shift in the deposition pattern. At sufficiently high forward speeds and flight heights, depending on the jet Reynolds number and ground clearance, the downwash influence near the ground can weaken, such that a fraction of droplets may no longer deposit directly with the downwash but instead remain suspended in the wake or be transported downstream [46]. In addition, ambient wind speed, turbulence intensity, and relative humidity regulate droplet evaporation, drift, and redistribution in the air. Previous studies have indicated that small droplets are more prone to off-target movement under low humidity and windy conditions, making them a primary source of spray drift risk [47].

2.2.2. Droplet Dynamics in UASS Downwash and Multiscale Drift Responses

After exiting the nozzle, droplet motion exhibits a pronounced coupling between velocity and size. Fritz et al. [11] reported that large droplets can retain high momentum over short distances, whereas fine droplets decelerate rapidly and tend to reside in low-velocity regions or be carried by turbulence, thereby forming spatial zones enriched in fine droplets. This phenomenon not only explains a potential source of bias whereby laser diffraction measurements may overestimate the fraction of fine droplets, but also underscores the necessity of explicitly accounting for size–velocity coupling in drift models [48]. Recent PIV studies have further elucidated the origin of this coupling from a flow-field perspective. Hu et al. [49] found that, as rotor speed increases from 0 to 1800 r·min^{-1}, the high-velocity region within the downwash expands substantially, and the droplet velocity distribution evolves from a dispersed pattern into a concentrated unimodal distribution, exhibiting a pronounced "velocity focusing effect." This effect enables a larger fraction of droplets to deposit on the target region at higher velocities, thereby enhancing deposition efficiency and reducing drift sensitivity to some extent.

At larger spatial scales, the wake vortex structures associated with different UASS configurations further modulate droplet transport pathways and drift behavior. Field experiments in vineyards conducted by Wang et al. [50] demonstrated that differences in downwash–wake structures among aircraft types lead to significant variation in airborne drift. Helicopter-type platforms, characterized by strong downwash, stable wake vortices, and large vertical extent, produced substantially higher drift levels than hexacopter and octocopter UASSs, whereas the hexacopter, with nozzles positioned closer to the rotor coverage zone, exhibited weaker droplet perturbation by the wake and consequently the

best deposition performance. Systematic tests based on INRAE's EoleDrift platform by Delpuech et al. [51] further indicated that UASS spraying typically presents a "near-ground drift structure," with 75–96% of drift occurring within 0–2 m above the ground, and high-altitude drift fractions being much lower than those of conventional airblast spraying. This characteristic arises from rotor downwash, which presses droplets toward the ground, resulting in a dynamic pattern of UASS spraying characterized by drift enrichment at low altitude (typically 1~2 m above the canopy or ground) and limited drift at higher altitudes (generally $\geq$3 m), as commonly used in experimental studies [50,52].

2.3. Droplet–Flow Coupling and Visualization Requirements

2.3.1. Multiscale Coupling Mechanisms Between Droplet Initial Conditions and Rotor-Induced Flow

The fluid dynamic characteristics of UASS spraying are jointly determined by three components: nozzle atomization, rotor downwash, and droplet transport, as shown in Figure 1. These components do not act as a simple superposition; rather, they form a highly coupled three-dimensional interaction system. The internal geometry of the nozzle plays a primary role in shaping liquid sheet breakup behavior, including Rayleigh–Plateau and aerodynamic sheet breakup modes, which in turn influence the spectral width and dominant range of droplet sizes. However, the resulting droplet size distribution is also modulated by formulation properties (e.g., viscosity and surface tension), nozzle–flow interactions, and operating conditions. Changes in nozzle operating pressure generally shift the droplet spectrum toward finer or coarser droplets, but this trend is contingent on the combined effects of liquid properties and flow conditions rather than a single breakup mechanism alone. Furthermore, the nozzle installation position determines the spatial overlap between the initial spray plume and the rotor coverage zone, thus influencing the dynamical response of droplets after entering the downwash region [24,28]. In typical commercial UASS configurations, nozzles are mounted within or slightly below the rotor disk, with installation distances on the order of tens of centimeters and injection directions approximately aligned with the downwash, which strongly affects the initial droplet–flow interaction. The rotor-induced flow further exerts a profound impact on droplet vertical transport paths, the distribution of the velocity field, and the redistribution process. These factors together constitute a typical "nozzle–airframe–flow-field" three-dimensional coupled influence model, which can explain why coarse-droplet nozzles (IDK/AIN) exhibit stronger anti-drift capability in UASS applications, while fine-droplet nozzles (XR/HCN) show high drift sensitivity under the combined effects of crosswind and wake vortices. While coarse droplets are often associated with reduced drift potential in conventional spraying, recent UASS studies indicate that spray performance cannot be explained by droplet size alone. Under rotor-induced downwash and dense canopy conditions, rotor–canopy interactions can substantially modulate droplet transport and deposition, allowing fine droplets to achieve effective canopy penetration in some scenarios [41].

The initial droplet size and exit velocity determine the response time scale and inertial settling capacity of droplets in the flow field [34]. From a physical perspective, this contrast can aslo be interpreted in terms of the droplet St, which governs the degree of droplet–flow coupling under rotor-induced flow conditions. Larger droplets (high St) tend to retain their momentum over short distances and penetrate the downwash to deposit directly, whereas fine droplets (low St) tend to reside in low-velocity regions and be transported by wake vortices or turbulence above the canopy, leading to redistribution. The rotor-induced flow exhibits a multiscale spatial structure [44], including the main downwash jet, tip vortices, and a wake recirculation zone. On the one hand, these structures enhance air exchange above the canopy and internal penetration, promoting droplet entry into the deeper canopy. On the other hand, they may also cause droplet uplift, residence, or

secondary drift. Existing studies have shown that, on typical octocopter and single-rotor platforms, droplet deposition patterns exhibit a certain spatial correspondence with vortex core regions. This height-dependent droplet–flow coupling structure is a key dynamical feature that distinguishes UASS spraying from ground boom and airblast spraying [44,45].

2.3.2. Necessity of Visualization-Based Monitoring

The UASS spraying process is essentially a highly transient, three-dimensional, strongly perturbed, and unsteady system. Immediately after leaving the nozzle, droplets are entrained, induced, and redistributed by the rotor-induced flow; their transport pathways vary on a millisecond time scale and span spatial scales from millimeters to meters. Traditional methods, such as water-sensitive paper, filter papers, and collection plates, can only record the final deposition pattern and cannot capture key dynamical information, such as droplet breakup, transport, intermediate residence, and vortex evolution. Point-wise wind speed measurement devices also struggle to resolve the steep velocity gradients and multiscale vortical structures beneath the rotor, and thus cannot support a systematic analysis of droplet–flow coupling mechanisms [44]. Therefore, accurately characterizing the true fluid dynamic behavior of UASS spraying necessarily relies on visualization-based monitoring methods capable of synchronously capturing the states of both droplets and the flow field. To faithfully reproduce the coupled process of "nozzle atomization–rotor disturbance–droplet transport–canopy redistribution," multimodal visualization techniques that concurrently acquire droplet size, velocity, spatial structure, and flow-field characteristics are required. Such methods provide an irreplaceable data foundation for spray mechanism studies, transport model development, drift assessment, and optimization of spraying parameters.

3. Visualization Monitoring Technology Framework for Spray Processes

According to Privitera et al. [53], spray measurement techniques can be classified into three categories based on methodological characteristics: intrusive methods, such as liquid immersion (LI) and water-sensitive paper (WSP), which obtain data by collecting or contacting droplets; non-intrusive methods, including PDPA, HSI, and laser diffraction (LD), which employ optical or laser systems for contactless measurement of the light field and droplet field; and machine-learning-based predictive tools, which use regression, neural networks, or other approaches to predict droplet properties and deposition patterns from existing experimental or imaging data. These three categories constitute the main technical framework for current spray measurement, from the perspectives of experimental intrusiveness and underlying physical principles.

Within this framework, recent research on visualization-based measurement of UASS spraying has developed a multimodal observation system centered on non-intrusive optical diagnostics, including optical imaging, laser scattering, and volumetric reconstruction, flow-field visualization, and multi-source data fusion, as shown in Figure 2. In essence, all of these belong to the family of non-intrusive imaging methods and enable an extension from two-dimensional droplet spectra to three-dimensional droplet fields and flow–spray coupled structures [54,55]. Because UASS spraying is characterized by strong three-dimensionality, strong transience, and strong perturbation, traditional intrusive sampling methods or point-wise flow measurements cannot reveal the dynamic evolution of droplet transport and flow-field structure. Therefore, this chapter focuses on this multimodal, non-intrusive measurement framework, discussing its imaging principles, technical characteristics, and suitability and limitations in UASS spraying research.

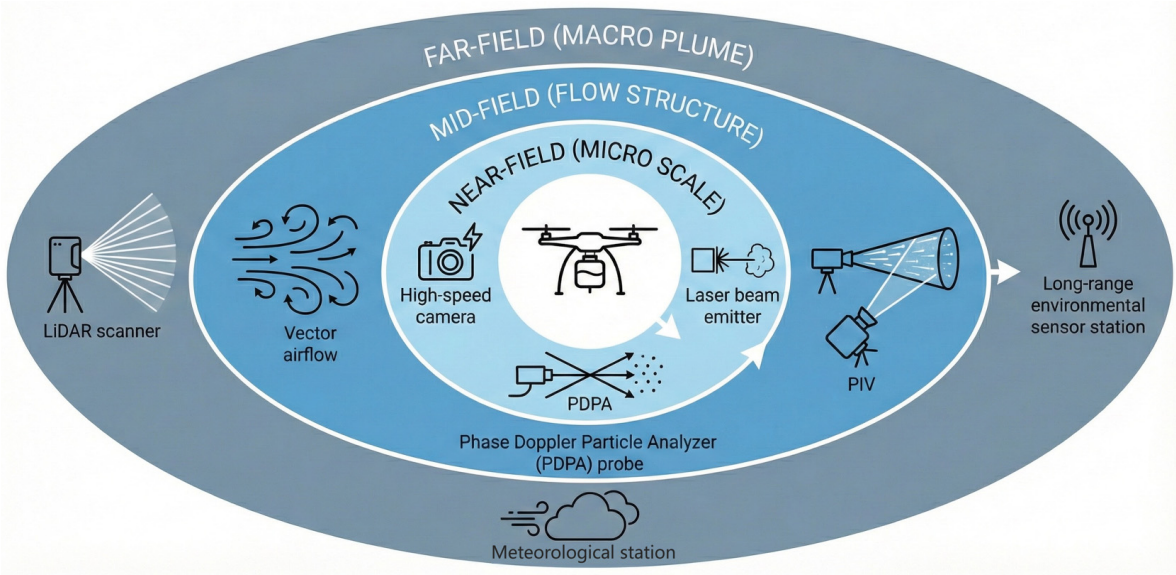


Figure 2. Multiscale Divided UASS Spray Monitoring Technology. The figure concept was assisted by the Gemini 3.0 AI model developed by Google LLC; the final illustration was manually produced using Microsoft PowerPoint.

3.1. Optical Imaging Visualization Techniques

Optical imaging techniques are among the earliest visualization methods to have formed a systematic framework in spray flow research. Based on their optical measurement principles, as summarized in Table 1. these methods can be divided into three major categories: scattering-based diagnostics, direct imaging techniques, and holographic interferometry methods. This classification clearly delineates the technological development pathway from point measurements to planar measurements and from two-dimensional to three-dimensional diagnostics. Their common feature is that they acquire droplet images or scattered-light-field signals and then use image-processing or signal-analysis techniques to quantitatively extract droplet-size distributions, velocity distributions, morphological features, and local spatial distributions.

Table 1. Comparison of optical imaging visualization techniques.

Subcategory	Representative Techniques	Measurement Dimension	Key Retrieved Information	Major Advantages	Main Limitations
Scattering-based diagnostics	PDPA, LDA/LDV	Point-wise	Droplet size distribution ($Dv_{0.1}$, $Dv_{0.5}$, $Dv_{0.9}$), velocity, RSF	High accuracy and repeatability; standardized reference for nozzle atomization and calibration	High cost; limited sampling volume; sensitive to alignment and droplet concentration; bias for non-spherical or air-entrained droplets
Direct imaging techniques	PDIA, high-speed imaging/shadowgraphy, PIV	Planar (2D)	Droplet size, morphology, spray angle, breakup dynamics, velocity fields	Intuitive visualization; flexible deployment; capable of resolving non-spherical droplets and flow–spray interactions	Strict requirements on focus and depth of field; reduced reliability in dense sprays; intensive post-processing
holographic interferometry methods	DIH, DHM, DHPIV	Volumetric (3D full-field)	Three-dimensional droplet size, spatial position, velocity, and dynamic evolution	Large depth of field; single-shot 3D reconstruction; suitable for dense and complex spray fields	High system complexity; heavy computational burden; stringent stability and calibration requirements

3.1.1. Scattering-Based Techniques

Scattering-based methods are point-wise diagnostics that obtain measurement information by detecting the intensity or phase difference in scattered light. They offer high accuracy and excellent dynamic response and are particularly suitable for quantitative analysis in the nozzle near-field and in sparse-spray regions. Typical representatives of this class of optical imaging techniques include PDPA and laser Doppler anemometers (LDA).

The PDPA employs two coherent laser beams that intersect to form a measurement volume and simultaneously retrieves droplet size and velocity from the phase difference in the scattered signal. It is a standard measurement method for nozzle near-field atomization. PDPA features high measurement accuracy and can simultaneously acquire droplet size, velocity, and relative span factor (RSF), making it well-suited for investigating the effects of nozzle type, spray pressure, and liquid physical properties on the initial conditions of atomization [56]. In early work, Nuyttens et al. [57] developed an automated nozzle characterization system based on PDPA, which performed three-dimensional scanning of nozzle spray fields in a climate-controlled chamber and could simultaneously obtain $Dv_{0.1}$, $Dv_{0.5}$, $Dv_{0.9}$, D_{32}, and RSF, among other characteristic indices. RSF was used to quantify droplet spectrum uniformity and later became an important parameter in ISO-based spray classification systems [58]. This method is a classical technique in quantitative two-phase flow measurements and has established a laboratory-standard basis for evaluating nozzle atomization performance.

Closely related to PDPA, LDA/LDV measures local velocity fields by using only the Doppler frequency shift in the scattered signal and is suitable for transient velocity measurements in gaseous phases or dilute liquid phases [59]. The two techniques share similar optical configurations and signal-processing principles, with PDPA adding a phase-detection module on top of LDA to enable joint measurement of droplet size and velocity.

In summary, scattering-based techniques are characterized by a high signal-to-noise ratio, strong repeatability, and traceable quantitative performance. They represent the most mature single-point optical diagnostic methods in spray measurement systems and provide the basis for data calibration and error referencing for subsequent direct imaging and wavefront reconstruction techniques.

3.1.2. Direct Imaging Techniques

This class of methods belongs to planar (areal) diagnostics. An optical imaging system captures spatial images of droplets or particles, and image analysis or related algorithms are then applied to infer physical quantities such as size, velocity, and morphology, thereby enabling visualization-based measurement. Representative techniques include PDIA, HSI/shadowgraphy, particle image velocimetry (PIV), and double-exposure imaging. By employing high-speed cameras to record the transient morphological evolution of spray breakup and atomization, these methods can directly reveal the spatial structure and dynamical characteristics of sprays [60].

PDIA is based on pulsed illumination and image recognition algorithms. It directly fits the drop size distribution using droplet image segmentation, identification, and statistical analysis. This technique can be applied in both near-field and far-field wind tunnel environments, offering good operational flexibility and shape recognition capability, and is particularly suitable for spray systems with relatively large droplet sizes [61]. Unlike PDA, which assumes droplets are nearly spherical, PDIA leverages digital imaging and automatic segmentation to compute size and morphology statistics for non-spherical droplets under appropriate depth-of-field and resolution conditions, while maintaining good repeatability in high-speed, fine-spray conditions. Compared with PDPA, PDIA shows good agreement in the medium and large droplet size ranges ($D > 25$ μm), whereas in regions with a high proportion of deformed droplets, PDPA underestimates volume fractions in the tail of the distribution due to the spherical assumption, while PDIA provides a more realistic characterization [17]. Therefore, PDIA and PDPA are complementary in nozzle near-field atomization studies, and PDIA is particularly suitable for regions near the nozzle orifice where strongly distorted, non-spherical droplets dominate.

HSI and shadowgraphy capture transient processes such as liquid sheet breakup, liquid bridge evolution, and ligament fragmentation by continuous high-frame-rate recording, and can directly reveal the temporal sequence and spatial structural evolution of liquid atomization. These methods typically employ backlighting and short-exposure imaging to obtain high-contrast silhouettes of droplets and liquid sheets, thereby enabling visualization of hole formation, sheet undulations, and droplet breakup mechanisms. When combined with phase-resolved illumination, dual-pulse synchronization, or infrared/fluorescence imaging, they can further quantify sheet thickness, droplet generation frequency, and breakup dynamics, providing key experimental evidence for the development of atomization models and the validation of numerical simulations [62,63].

Particle image velocimetry (PIV) is widely used for quantitative investigations of spray and flow-field characteristics. This technique acquires image sequences containing tracer particles via multiple exposures and uses cross-correlation algorithms to compute velocity vector fields. It can accurately describe velocity decay, wake vortex structures, and local recirculation features in sprays and rotor downwash flows, thereby supporting the elucidation of droplet penetration and redistribution mechanisms [64,65]. In contrast to HSI, which focuses on process visualization, PIV emphasizes quantitative computation of the flow field. In atomization research, PIV is often used in conjunction with smoke visualization or infrared imaging to identify canopy disturbances and turbulent structures, thereby revealing the mechanisms of droplet penetration and redistribution. De Cock et al. [66] further developed a high-speed double-exposure shadowgraphy system based on a PIV camera and pulsed LED illumination, enabling simultaneous measurement of droplet size and velocity. They introduced focus-based filtering and volume-weighted correction methods, effectively reducing defocus and sampling-volume biases. For ISO 25358 standard nozzles, results showed that the difference between this method and PDPA in Dv_{50} was less than 5%, although systematic deviations in Dv_{10} and Dv_{90} led to slightly larger RSF values, providing a feasible, low-cost alternative to PDPA and LDS.

3.1.3. Holographic Interferometry Methods (Wavefront Reconstruction Techniques)

Holographic interferometry methods (Holographic/wavefront reconstruction optical imaging techniques) are three-dimensional visualization methods. Their basic principle is to record interference fringes (holograms) formed by the object beam and reference beam, and to reconstruct the optical field using numerical algorithms to recover three-dimensional spatial information of the object [67]. Compared with conventional two-dimensional imaging, holographic interferometry not only provides droplet morphology and spatial distribution, but also enables three-dimensional quantitative reconstruction of droplet size, position, and dynamic evolution [68]. These methods offer high spatial resolution and full-field measurement capability, and can achieve complete three-dimensional reconstruction of particles or droplets in complex multiphase flows from a single exposure. Representative techniques include digital holographic microscopy (DHM), digital holographic interferometry (DHI), DIH, and digital holographic particle image velocimetry (DHPIV).

DHM is mainly used for microscale studies and can reconstruct droplet morphology, refractive index, and evaporation dynamics with high accuracy, making it suitable for phase-change processes and microstructural observations. DHI compares holographic phase changes at different times or under different states to achieve highly sensitive quantitative measurements of droplet evaporation, condensation, and local refractive index variations, and can be used for dynamic characterization of temperature and density fields. DIH records interference holograms generated by droplets and the reference beam, and numerically reconstructs intensity fields at different depth planes, thereby obtaining three-dimensional distribution information (size, position, velocity) of droplet ensembles

from a single exposure and effectively overcoming the depth-of-field limitations of conventional imaging [69]. DHPIV combines holographic imaging with principles of particle velocimetry, using time-resolved reconstructions to compute flow-field velocity vectors, thereby enabling full-field, quantitative measurement of three-dimensional droplet motion in sprays and multiphase turbulence [70]. These methods offer significant advantages in droplet visualization research, including high spatial resolution, full-field three-dimensional reconstruction, and dynamic process capture. However, their practical applicability varies substantially: DHM and DHI are primarily restricted to laboratory-scale or wind-tunnel environments due to stringent optical stability and alignment requirements, whereas DIH and DHPIV exhibit greater potential for UASS-relevant measurements but remain mostly limited to controlled or semi-controlled conditions.

In recent work, Kumar et al. [55] proposed a three-dimensional spray visualization framework based on DIH, incorporating a modified U-Net and VGG-16 combination to achieve fully automated 3D droplet field segmentation and noise removal. The method maintained stable performance across different nozzle types, droplet size ranges, and high-density spray conditions, and achieved high-accuracy detection of droplet size, position, and velocity in the 20–500 μm range. Compared with laser diffraction (LD) techniques, the median diameter $Dv_{0.5}$ obtained by machine-learning-based DIH (ML-DIH) showed excellent agreement with NIST standard values, whereas LD is prone to systematic errors (settling bias) due to differences in droplet settling velocities, leading to underestimation of large droplets. These results indicate that holographic interferometry techniques have significant advantages in three-dimensional measurement and dynamic reconstruction of multiscale droplet fields. Despite these advances, current DIH-based frameworks are still mainly validated under controlled experimental conditions, and their application in open-field UASS operations remains challenging due to platform vibration, ambient light variability, and limited measurement volume.

In recent years, smart devices and cloud computing have also been introduced into spray visualization. These approaches are not intended for in-flight spray visualization, but rather serve as pre-flight nozzle inspection and off-line quality control tools that complement UASS spray monitoring by ensuring nozzle integrity and spray pattern consistency prior to operation. Carreira et al. [71] proposed a rapid nozzle inspection framework based on smartphone imaging and cloud processing, in which spray images are captured by a mobile phone and processed in the cloud to achieve non-intrusive characterization of spray angle, spray pattern distribution, and solid jets. The method uses automatic threshold segmentation, Canny edge detection, and Hough transform to extract spray angle, yielding a mean absolute error of approximately 4.45° and a relative error of about 4%, and can identify "degraded nozzles" that fall outside the ISO 5682-1 tolerance range. For spray pattern analysis, grayscale profiles are extracted to distinguish the unimodal distribution of flat-fan nozzles from the bimodal distribution of hollow-cone nozzles and to automatically identify solid jets [72]. This study demonstrates the feasibility of smartphone imaging as a nozzle quality screening tool, facilitating nozzle maintenance and pre-operation quality control directly in the field. Kumar et al. [55] combined laser diffraction (LDA) with image analysis software, including DepositScan, ImageJ, and Dropleaf, to establish baseline droplet-spectrum data. Their results showed that VMD and NMD measured in ImageJ exhibited the highest consistency with LDA results ($R^2 > 0.9$), and they proposed a field-applicable standardized droplet-spectrum analysis framework based on "LDA calibration + image batch processing," providing a practical solution for rapid UASS droplet characterization.

Overall, optical imaging methods are characterized by high spatial resolution, intuitive visualization, and strong suitability for mechanism-oriented studies, but most holographic

techniques remain primarily suited to nozzle near-field investigations, wind-tunnel experiments, or standardized characterization setups rather than routine UASS field deployment. In UASS scenarios, their primary contribution lies in establishing reliable initial boundary conditions and providing droplet size and velocity inputs for subsequent droplet–flow coupling models.

3.2. Laser Scattering and Volume Reconstruction Technologies

Laser scattering and volumetric visualization techniques enable quantitative characterization of droplet ensembles or plumes over a larger spatial extent. Representative methods include laser diffraction systems (LDS), laser imaging and light-sheet techniques, as well as LiDAR and three-dimensional reconstruction, as shown in Table 2. These techniques use droplet-induced scattering, diffraction, or reflection of laser light as information carriers and can directly provide droplet distributions, drift distances, and plume geometric characteristics, serving as key tools for three-dimensional quantification of spray performance.

Table 2. Comparison of laser scattering and volumetric reconstruction techniques.

Subcategory	Representative Techniques	Spatial Scale	Key Retrieved Information	Major Advantages	Main Limitations
LDS	Laser diffraction analyzers	Local/statistical	Volumetric droplet size distribution (Dv metrics)	High degree of standardization; rapid measurement; large statistical sample size	Systematic bias for non-spherical or air-filled droplets; overestimation of fine droplets at low airspeeds
Laser imaging and light-sheet techniques	Scattered-light imaging, line-laser scanning, 3p-SLIPI	Planar to quasi-3D	Drift index (DIX), plume height, drift distance, surface-area mean diameter (D_{21})	High sensitivity to drift behavior; strong correlation with field deposition measurements	Susceptible to ambient light and background aerosols; requires cross-calibration
LiDAR and three-dimensional reconstruction	Scanning LiDAR, multi-line laser scanners, line-laser–camera systems	Large-scale 3D	Three-dimensional point cloud density, plume geometry, drift potential indices	Large measurement range; real-time, non-intrusive plume monitoring; well suited for UASS field studies	High equipment cost; limited sensitivity to very fine droplets; complex point-cloud interpretation

3.2.1. Laser Diffraction Systems

Laser diffraction techniques are based on Mie scattering principles. By analyzing the angular distribution of scattered light intensity, they can compute the volumetric droplet size distribution and rapidly obtain droplet-spectrum information. With a high degree of standardization, they serve as a benchmark method for evaluating nozzle atomization performance. However, systematic biases arise in the presence of air-entrained droplets, non-spherical droplets, and substantial velocity differences. Fritz et al. [11] systematically investigated the influence of laser diffraction measurement conditions on droplet spectra and found that, due to velocity differences among droplets of different sizes, LDS significantly overestimates the fraction of fine droplets at low wind speeds (<6.7 $m \cdot s^{-1}$), with V < 100 μm volume fractions being overestimated by a factor of 2–3, leading to underestimation of $Dv_{0.1}$. By combining PIV and shadowgraphy measurements, the study established a quantitative correction relationship between spatial sampling and temporal sampling and proposed standard measurement conditions, thereby providing a basis for cross-laboratory consistency and standardization of spray droplet spectra.

3.2.2. Laser Imaging and Light-Sheet Techniques

Laser imaging techniques capture scattered light from droplet ensembles and extract grayscale, centroid, and boundary features to construct indices, such as the drift index (DIX) and the characteristic height. Related studies have shown that the correlation coefficient between these indices and passive field sampling can exceed 0.9, with drift distance prediction errors below 6%. These methods demonstrate high quantitative reliability in wind tunnel and ground-based field and have become important tools for rapid

assessment of spray drift. In high-optical-thickness sprays, multiple scattering can significantly affect the quantitative interpretation of scattering signals. Stiti et al. [73] introduced three-phase-shift structured laser illumination (3p-SLIPI) into a polarization-ratio-based sizing system and used a telecentric lens to fix the scattering angle, thereby spatially filtering multiple-scattering signals. In dense sprays with an optical depth of up to 3, they obtained high-accuracy distributions of the surface-area mean diameter (D_{21}), with correlation coefficients above 0.93 compared with PDI measurements, demonstrating the potential of polarization imaging for visualizing complex spray fields. However, polarization-based techniques such as 3p-SLIPI currently require stringent optical alignment and controlled illumination conditions, which substantially limit their direct deployment in field-scale UASS experiments subject to platform vibration, motion, and variable ambient light.

3.2.3. LiDAR and Three-Dimensional Reconstruction

LiDAR is one of the key techniques for three-dimensional visualization of spray plumes. Gil et al. [74] proposed a ground-based scanning LiDAR framework for drift measurement using an SICK LMS-200 to construct dynamic point clouds of spray clouds. They extracted indices such as maximum height, maximum length, centroid position, and point cloud density, capturing the temporal and spatial evolution of cloud diffusion, uplift, and canopy detachment at a time resolution of 0.1 s, and thereby demonstrating the potential of LiDAR for non-contact, time-resolved characterization of spray plume dynamics. LiDAR measurements showed that nozzle type and airflow rate have significant effects on the drift cloud structure in orchards: conventional hollow-cone nozzles produced dense, widely spread drift clouds, whereas air-induction hollow-cone nozzles generated point clouds with markedly lower density and reduced drift extent. Building on this, Zheng et al. [19] proposed a spray distribution detection method based on multi-line laser scanning. By temporal stacking and noise suppression, they achieved three-dimensional reconstruction of droplet plumes and quantified the spatial distribution of spray and the effective swath width in real time, with results in good agreement with water-sensitive paper data, marking a transition from "two-dimensional measurement" to "volumetric reconstruction." Wang et al. [75] further proposed a three-dimensional droplet reconstruction method using 2D LiDAR combined with vertical scanning motion. Through dual ground-plane fitting, point cloud rotation correction, noise removal, and triangulated mesh reconstruction, they achieved rapid three-dimensional visualization of air-assisted spray droplet clouds and revealed the coupled influence of nozzle mounting height and fan speed on the spatial structure of droplet clouds.

For UASS scenarios, Wang et al. [54] developed a three-dimensional visualization method for droplet distribution based on synchronized line-laser and camera acquisition. By allowing the UASS to vertically scan the laser plane at a constant speed and mapping the time axis onto a spatial coordinate, they reconstructed the three-dimensional point cloud density field of the droplets. Droplet recognition was performed using a color index $(R - B)/(R + G + B)$, combined with background modeling, denoising, and random down-sampling to normalize point cloud density. Without dedicated LiDAR hardware, this approach enables low-cost, high-spatial-resolution three-dimensional measurements. Comparison of the reconstructed 3D point clouds with CFD flow fields showed that, for different rotor configurations, the outward expansion directions, boundary morphology, and diffusion trends of droplet clouds agreed closely with simulation results, indicating that light-sheet laser scanning can serve as a mesoscale complementary technique to LiDAR. Compared with near-field imaging, laser scattering techniques overcome limitations in measurement scale and achieve a leap from two-dimensional images to three-dimensional volumes. Their limitations include high equipment costs, insensitivity to droplet size

distributions and fine droplets, as well as sensitivity to ambient light, atmospheric aerosols, and signal attenuation under dense spray plumes; nevertheless, they offer irreplaceable advantages for UASS long-distance drift monitoring, multi-platform comparison, and buffer zone delineation. For UASS, LiDAR, and line-laser scanning methods are particularly suitable for field drift monitoring, comparing different UASS configurations, and optimizing buffer strip width, thereby providing essential support for environmental risk assessment in UASS spraying scenarios.

3.3. Standardization Challenges in Multisource, Flow–Spray Fusion Visualization and Measurement

Rotor-induced flow is the core driving force behind UASS spray transport and deposition behavior. Synchronous observation of airflow velocity fields, vortex structures, and droplet clouds is therefore crucial for understanding the full "flow–spray–target" pathway. In recent years, multisource fusion visualization techniques have developed rapidly. By synchronously acquiring droplet and flow-field data within a single spatiotemporal framework, they have established a continuous observation chain covering the nozzle near-field, rotor flow field, and field deposition. Studies have shown that, by using synchronized triggering and temporal registration, sensors such as PDIA, HSI, PIV, and LiDAR can be jointly applied to obtain spatiotemporal mappings between droplet distributions and flow-field structures [24]. Multisource observations indicate that deposition hotspots often spatially coincide with rotor-induced vortex cores or high-shear regions, and that as downwash intensity or external wind disturbance increases, deposition zones shift downstream and become more concentrated. In contrast, drift clouds are more likely to form in the outer regions of vortices or on the outer side of shear layers. Such fused observations not only reveal the regulatory mechanisms of rotor flow on droplet transport pathways but also facilitate the development of a standardized visualization framework for UASS spraying, gradually forming a continuous validation chain with cross-validated indicators across wind tunnel, field, and simulation platforms.

However, because different measurement techniques are based on different physical principles, they exhibit non-negligible systematic biases in droplet spectrum and flow-field observations. Recent cross-method studies have shown that different measurement principles introduce stable biases in droplet size, volume distribution, and velocity measurements. Privitera et al. [76] conducted a systematic comparison of liquid immersion (LI), laser diffraction (LD), phase Doppler (PDPA), and shadowgraphy (SG) and found that, under fine-spray conditions ($Dv_{50} < 400$ μm), these methods exhibit relatively high consistency for $Dv_{0.5}$, whereas under coarse-droplet and non-spherical droplet conditions, deviations increase substantially. LD tends to yield smaller size estimates, followed by SG; PDPA tends to overestimate number-based and characteristic diameters (D_{10}, D_{20}, D_{30}, $Dv_{0.5}$), while LI generally overestimates D_{32} and volumetric distribution parameters ($Dv_{0.1}$, $Dv_{0.5}$, $Dv_{0.9}$). Sijs et al. [77] compared image analysis, PDPA, and LD and reported that the three methods show good agreement under fine-spray conditions, but deviations increase markedly for coarse or non-spherical droplets. PDPA may misclassify air-entrained droplets as small droplets, whereas LD may produce "pseudo-large droplets" due to distribution fitting assumptions. Privitera et al. [53,76] further noted that multiple scattering, limited depth of field, evaporation, and droplet coalescence all affect the consistency between LD and PDPA and require mitigating measures, such as constant-humidity environments, oil-based media, or multi-angle scattering corrections. Overall, systematic biases among measurement methods are influenced not only by droplet size, morphology, and air entrainment but also by flow velocity, optical path, scattering angle, and imaging conditions. Recognizing these biases is a prerequisite for improving cross-platform comparability and standardization.

From an integrated application perspective, different measurement methods exhibit distinct strengths in spray research. PDPA and LD, owing to their high degree of standardization and repeatability, are key tools for standardized nozzle evaluation and baseline droplet spectrum testing [34,57]. PDIA, HSI, and DIH are more advantageous for elucidating near-field atomization mechanisms, non-spherical droplets, and breakup processes [55]. LiDAR and laser scanning are better suited for characterizing the three-dimensional structure of large-scale spray plumes [78], while PIV is the core technique for capturing rotor flow vortex structures and turbulence characteristics [79]. Because UASS spraying involves a continuous coupling chain of "nozzle atomization–rotor flow field–field deposition," no single measurement technique can fully describe its cross-scale characteristics. Consequently, establishing standardized and aligned frameworks across methods has become an important trend in spray visualization research.

Current studies commonly employ standard nozzles and reference droplet spectra as unified benchmarks. By calibrating and aligning outputs from different techniques such as PDPA, LD, DIH, and LiDAR, they gradually construct a multimodal feature system compatible with droplet size, velocity, plume structure, and temporal dynamics [55]. Such fusion-based models not only help offset systematic biases across measurement techniques but also provide a foundation for cross-validating indicators across wind tunnel, field, and numerical simulation platforms, making "multisource-consistent, cross-platform-comparable" data chains feasible [78,80]. An overview of the strengths, limitations, and suitable application contexts of different visualization monitoring technologies is provided in Table 3. Looking ahead, multimodal fusion and cross-platform standardization will become key research directions in UASS spray visualization and will form the critical basis for building unified, reproducible spray measurement systems and dynamical models [24].

Table 3. Comparison and applicability analysis of visualization monitoring technologies in the spraying process.

Technology Category	Measurement Principle and Key Indicators	Typical Application Scenarios	Advantages and Representative Results	Limitations and Improvement Directions
PDPA	Laser beam crossing area; calculates droplet size and velocity from phase difference in scattered signal, simultaneous acquisition of droplet size spectrum and velocity spectrum.	Near-field of nozzle, climate chambers, wind tunnels	High accuracy, good reproducibility; standard method for nozzle atomization and reference nozzle calibration [57].	Expensive equipment, sensitive to alignment and particle concentration, limited measurement volume; bias in measuring gas-phase, non-spherical droplets.
PDIA	Uses pulse light source and high-speed imaging to segment and count droplet images, directly identifying droplet size and number density.	Laboratories, wind tunnels, near-field and outer field near nozzle	Flexible operation, moderate cost; can identify non-spherical and gas-containing droplets; results consistent with PDPA in the mid-size range [81].	High requirements for focus and depth of field management; small droplets are susceptible to noise interference; for high-concentration spray fields, threshold and focus criteria need to be combined.
HSI/Shadowgraphy	Continuous frame capture of liquid film breakage and droplet formation process, extracting breakage time, liquid bridge evolution, spray angle, etc.	Atomization mechanism research, centrifugal nozzle performance analysis	Intuitive display of liquid film rupture, aggregation, and reatomization processes; supports breakage model validation [66].	Sensitive to lighting, background, and focus conditions; high post-processing workload; precise calibration needed for droplet size quantification.
DIH	Records holograms of droplet clusters and reconstructs different depth planes to obtain 3D droplet size and location distribution.	High-concentration spray fields, complex droplet cluster structures, UASS local 3D measurements	Large depth of field, complete volume information; combined with deep learning, high precision measurements in the range of 20–500 μm, overcoming LD settling bias [55].	Large computational requirements for reconstruction, high demands on system stability and calibration; large-scale application requires calculation acceleration.
LD	Based on Mie scattering, measures scattering angle intensity distribution and inverts volume distribution.	Nozzle laboratory benchmark testing	Highly standardized, fast measurement speed, large statistics; commonly used for nozzle classification and droplet spectrum comparison [11].	Insufficient accuracy for gas-phase, non-spherical droplets; overestimates fine droplet proportion in cases with speed differences and low wind speed.
Laser Imaging	Captures scattered light images of droplet clusters, extracts grayscale centroids and boundaries, constructs drift index (DIX) and characteristic height.	Wind tunnel and field drift assessment	Can quantitatively characterize drift rate, drift height, and distance; high correlation between DIX and deposition rate ($R > 0.9$).	Affected by ambient light and background aerosols; needs mutual calibration with sampling methods and LD/PDPA results.
LiDAR	Emits pulse laser and receives echo to construct pseudo-3D/3D point cloud fields.	Wind tunnels, fields, large-scale drift monitoring, buffer zone evaluation	Large range, high spatial resolution, real-time drift potential monitoring (DP, DPRP), can differentiate nozzle and airflow differences [74]	Expensive; only sensitive to "surface clouds"; small droplets and far-side clouds are easily blocked; sensitive to humidity and aerosols, data interpretation is complex.
Laser Scanning (Line Laser + Camera)	Laser line forms 2D cross-section; UASS or sprayer moves according to planned trajectory, reconstructing 3D cloud via time-space mapping.	Three-dimensional droplet distribution, spray width structure analysis	Simple hardware, low cost, high spatial resolution, consistent with CFD wind field; can supplement LiDAR for medium-scale analysis [54].	Limited sensitivity to droplet size; high-power lasers pose safety risks; requires optimization of angle and background obstruction.
PIV	Tracks tracer particle displacement, calculates velocity vectors and vorticity fields.	Rotor wind fields, canopy disturbances, wind tunnel validation	Visualizes downward flow and vortex structures, reveals interactions between wind fields and droplets; can be verified with CFD.	Tracer placement is complex, applicable range limited by field of view and optical conditions; difficult to cover large-scale fields.
Multi-source Fusion Visualization	Synchronously triggers PDIA/high-speed imaging and PIV/LiDAR to achieve spatiotemporal registration and data fusion.	Wind tunnel-field integrated research, wind-droplet-target coupling analysis	Monitors the entire process from droplet-wind-field-deposition, revealing spatial correspondence between deposition hotspots and vortex structures.	System synchronization and data fusion algorithms are complex; high hardware and computational power requirements.
Field Rapid Detection (Smart Terminals)	Uses smartphones or portable devices to capture spray images, analyzing spray angles, spray width, and nozzle consistency.	Field quality control, pre-operation inspection, nozzle screening	Portable and quick, low cost, suitable for equipment quality inspection and rough state evaluation [71].	Limited accuracy, suitable only for geometric and pattern detection, difficult to provide standardized droplet size data.

4. UASS Spray Visualization Practice and Applications

4.1. Experimental Platform Validation: From Wind Tunnels to Controlled Environments

The core value of wind tunnels and controlled-environment experimental platforms in UASS spray research does not lie in the "high-precision measurement" capabilities of individual devices, but in their ability to provide a set of controllable, repeatable, and comparable experimental boundary conditions for the complex droplet-flow coupling process [25]. By decoupling factors such as nozzle atomization, airflow shear, and canopy disturbance under controlled conditions, these platforms establish a "physical baseline layer" for subsequent drift models, CFD simulations, and evaluations of drift-reduction technologies [65]. At the nozzle near-field scale, small cross-section wind tunnels combined with PDPA, laser diffraction (LD), PDIA, HSI, and DIH can unify boundary conditions such as initial droplet size, velocity, and spray angle [55]. Hydraulic nozzles typically produce broad droplet spectra with a high fraction of fine droplets and exhibit strong sensitivity to incoming flow disturbances at low wind speeds. In contrast, centrifugal nozzles yield more concentrated size distributions and allow continuous control of $Dv_{0.5}$ via disc speed or PWM, with deposition profiles below the nozzle exhibiting parabolic decay and sometimes showing local "reverse deposition bands" due to vibration or recirculation. Similar structures can also be observed in UASS downwash flows [18]. This shift is reflected in three core aspects, corresponding to the near-field, mid-field, and far-field integration framework illustrated in Figure 2 (Section 3): (i) near-field reconstruction at the nozzle scale, where parameterized boundary conditions such as droplet size distribution and initial velocity are established; (ii) mid-field representation of coherent flow and plume structures driven by rotor–canopy interactions; and (iii) far-field modeling of spray plume transport and dispersion, typically addressed through data-driven or learning-based predictive models built on multimodal visualization data, with each level operating at progressively larger spatial and temporal scales.

Wind tunnel experiments have also revealed systematic discrepancies between nozzle geometry and the actual spray geometry. Standardized tests have shown that, under dynamic operating conditions, the actual spray angle of many nozzle types can deviate by about 10% from the nominal value, and that an increase in spray angle is accompanied by thinning of the liquid sheet and a reduction in $Dv_{0.5}$, indicating a trend toward finer atomization [35]. This implies that, even when pressure and flow rate are identical, nozzle mounting orientation, boom vibration, and incoming-flow shear can still modify the downstream droplet spectrum and coverage pattern by influencing the "effective spray angle." In UASS with strong rotor downwash, using spray angles measured under static water conditions or catalog values as model inputs is likely to underestimate the proportion of fine droplets and drift risk in edge regions. In addition, multi-technique comparisons on wind tunnel platforms have demonstrated systematic differences among measurement methods. Tri-modal experiments combining PIV, shadowgraphy, and LD have shown that, at low wind speeds or when droplet size–velocity differences are large, spatially sampled LD substantially overestimates the fraction of fine droplets, leading to underestimation of $Dv_{0.1}$, whereas temporally sampled PDPA is closer to the true mass distribution [11]. This indicates that wind tunnel measurements do not represent absolute ground truth; different measurement principles must be calibrated with respect to flow conditions, or structural biases may be introduced into spray models.

At mid- to far-field scales, large-section or semi-open wind tunnel platforms can introduce crosswind, rotor downwash, and artificial canopies to systematically elucidate the coupling mechanisms among the nozzle, the flow field, and the canopy. Typical studies employ LiDAR, laser imaging, PIV, or anemometer arrays to simultaneously record plume morphology, velocity fields, and canopy motion. Results have shown that plume character-

istic height increases with incoming wind speed, while drift potential decreases markedly as median droplet diameter increases. When an artificial canopy is introduced, recirculation and toroidal vortices at the canopy top substantially alter deposition pathways, making fine droplets more prone to uplift and the formation of resuspension zones downstream. This behavior closely matches field observations of combined "near-ground drift + localized uplift" patterns [18]. In contrast to traditional wind tunnels with "fixed nozzle + steady inflow," new-generation UASS-controlled platforms place greater emphasis on the combined action of rotor-induced flow and crosswind. For example, UASS simulators that couple a nozzle–rotor module with an external flow field can scan the effects of different wind speeds, angles of attack, and nozzle layouts at relatively low cost [25]. Going further, two-phase UASS spray platforms that integrate real aircraft (e.g., DJI T30), adjustable rotor speeds, and PIV light sheets enable synchronous visualization of downwash flow fields and droplet transport, and allow quantitative characterization of the relationships among vortex structures, downwash intensity, and droplet velocity fields [49]. Collectively, these results indicate that UASS spray experimental systems are evolving from "nozzle-dominated" toward "integrated rotor–nozzle" configurations, and that platform roles are shifting from "airflow supply devices" to "composite flow-field simulators."

In terms of drift metric quantification, line-laser imaging in wind tunnels combined with image-feature-based regression models provides an important pathway for non-contact, consumable-free drift evaluation. Optical features of spray clouds—such as grayscale centroid, position of maximum grayscale, and horizontal/vertical mean grayscale—can be significantly correlated with drift rate, characteristic height/distance, and the drift potential index DIX as defined in ISO 22856 [82] and GB/T 32241-2015 [83]. Correlation coefficients typically exceed 0.9, and the relative errors in characteristic height and distance can be controlled to around 1% [84]. This demonstrates that, in standardized wind tunnels, active optical signals can serve as substitutes or front-end screening tools for traditional sampling metrics, providing a technical basis for future high-throughput screening systems of nozzle–parameter combinations.

Overall, wind tunnel and controlled-environment platforms provide three core forms of support for UASS spray research. First, at the nozzle near-field level, they unify initial boundary conditions, such as droplet size, velocity, and spray angle, thereby establishing a comparable basis for nozzle selection and droplet-spectrum modeling. Second, at the composite flow-field level, they decouple and quantify the effects of rotor downwash, crosswind, and canopy disturbance on plume structure and drift behavior, constructing a continuous experimental chain from atomization to plume dispersion. Third, at the indicator-system level, multi-method comparisons and regression mappings gradually form a standardized quantitative framework linking droplet size, velocity, drift indices, and spatial distributions. It must be critically noted, however, that current controlled platforms remain limited by assumptions of flow steadiness, incomplete reproducibility of turbulent structures, and scaling issues. Wind tunnel flows often struggle to reproduce the non-stationary turbulence and thermal stratification of field conditions, and the three-dimensional interactions among rotor, ground, and canopy are inevitably "compressed." Therefore, wind tunnels and controlled-environment platforms are better suited as tools for mechanism verification and model calibration than as direct bases for deriving operational parameters and safety distances. The applicability of various agricultural spraying test platforms is summarized in Table 4.

Table 4. Comparison of agricultural spraying test platform types and their applicability.

Platform Type	Typical Operating Conditions and Scenarios	Observable Indicators	Advantages	Limitations	Representative References (Examples)
Standard Wind Tunnel (Small Cross-section)	Fixed nozzle/small spray bar, conducting droplet spectrum and drift testing under controlled wind speed, temperature, and humidity.	Droplet size distribution, lateral distribution, near-field drift amount.	Controlled conditions, high repeatability, suitable for single-factor analysis.	Limited space, difficult to replicate UASS scale and rotor wind fields.	Liu et al., 2021 [85]
Semi-open/Large Wind Tunnel (EoleDrift, etc.)	Artificial orchard obstacles installed, UASS/airblast tested under forced crosswind to assess drift height distribution and drift reduction techniques.	Height distribution, total drift index, nozzle/height comparison.	Simulates real orchard conditions in a controlled environment with unified evaluation metrics.	Expensive equipment, fixed spatial layout, limited representativeness for complex terrain.	Delpuech et al., 2022 [51]
Artificial Orchard + Field Trials	Artificial vineyard or simulated fruit tree clusters, UASS low-altitude spraying with various types of samplers set up.	Canopy deposition, ground settlement, airborne drift, mass conservation.	Balances controlled structure with field wind environment, suitable for mass balance analysis.	Incomplete meteorological control, long trial period, high labor costs.	Wang et al., 2021 Cui et al., 2025 [50,86]
Field Trials (Natural Orchards/Farmland)	UASS or spray bar spraying at real orchards or farmlands, deposition boards and drift sampling lines set up.	Deposition, drift distance, and distribution under real operational conditions.	Closely mimics actual production conditions, results directly applicable to technical promotion evaluation.	High meteorological randomness, poor repeatability of trials; difficult to analyze fine mechanisms.	Shi et al., 2024; Wang et al., 2019 [87,88]
LD/PDPA Indoor Droplet Size Test Bench	Droplet size testing under standard nozzles, fixed pressure, and flow conditions.	$Dv_{10/50/90}$, RSF, droplet spectrum variations.	Mature technology, high accuracy, basis for nozzle calibration and droplet spectrum comparison.	Cannot provide spatial structure and wind field effects; difficult to directly extrapolate to UASS rotor scenarios.	De Cock et al., 2016 [66]
HSI/DIH Optical Platform	Visualizes liquid film breakage, droplet formation, and local 2D/3D field distributions in a small range.	Droplet size, speed, 3D position, local droplet morphology.	Can analyze breakage mechanisms and local dynamics, supports ML/AI analysis.	Limited field of view, difficult to cover entire spray width or large-scale drift.	Kumar et al., 2024 [55]
LiDAR 3D Scanning Platform (Ground-mounted)	LiDAR installed at fixed locations, scanning airblast or orchard sprayer drift plume in real-time.	Plume shape, width, central position, relative concentration.	Long-range, non-contact, real-time measurement without interfering with spray process.	Limited sensitivity to small droplets and low-density clouds; measures only "surface clouds."	Gil et al., 2013; [74]
LiDAR + Motion Scanning (3D Reconstruction)	Spray machine or LiDAR moves via mechanical motion/operation to complete volume scanning and obtain 3D point cloud.	Three-dimensional point cloud, droplet cloud surface, spatial distribution.	Large-scale 3D droplet cloud measurements, suitable for analyzing wind-blown structures and nozzle position effects.	Complex data processing, high synchronization and registration accuracy requirements.	Wang et al., 2023 [75]
Laser Slicing Imaging + UASS Scanning	Laser line forms 2D cross-section, UASS moves according to planned trajectory to reconstruct 3D cloud field.	Three-dimensional point cloud, relative density, structural differences in machine types.	Relatively simple hardware, suitable for UASSs, high spatial resolution.	Limited droplet size sensitivity, high-power lasers require safety protection.	Wang et al., 2024 [54]
X-ray Imaging Test Bench	X-ray source and detector arranged in a controlled site to observe spray flow after penetrating canopy.	Mass flux, penetration rate, post-target drift risk.	Strong penetration capability, can directly quantify mass drift and canopy penetration.	Expensive equipment, high safety requirements, unsuitable for large-scale and routine applications.	Heindel, 2018; Qiu et al., 2023 [89,90]
UASS-specific Composite Platform (Wind Tunnel + Rotor + Crosswind)	UASS fixed or partially moving, applying crosswind and rotor downwash in the wind tunnel.	Drift amount under composite wind fields, height distribution, pressure/wind speed interaction.	Controlled conditions, includes real rotor effects, important for UASS drift mechanism research.	Limited space, machine and parameter combinations still need simplification; difficult to fully represent field unstable wind fields.	Zhang et al., 2023; Liu et al., 2023 [91,92]

4.2. Field-Scale Visualization: From Plume Structure to Target Deposition

Field environments comprise unsteady wind fields, complex terrain, and heterogeneous canopies, together forming a typical "rough boundary layer" with uncertainties far exceeding those in controlled settings. Consequently, the primary task of field visualization is no longer to finely disentangle the microscopic mechanisms of droplet–flow interactions, but rather to address two key engineering questions: Where does the spray ultimately go under real operating conditions? And can the resulting visualization evidence support buffer zone design, operational limits, and risk assessment? With the development of active optical technologies such as LiDAR, laser imaging, and X-ray diagnostics, these tools are gradually evolving from auxiliary observation methods into core measurement instruments for field drift assessment, while simultaneously revealing additional application boundaries and limitations in real-world conditions.

For monitoring the three-dimensional structure of plumes, fixed or mobile LiDAR systems have become central tools in field drift observation. LiDAR can continuously record the lateral expansion, width, peak position, and centroid trajectory of spray clouds over tens of meters, effectively compensating for the limitations of passive samplers such as WSPs and deposition plates, which capture only endpoint information. Numerous studies have shown that integrated LiDAR return signals exhibit good linear relationships with deposition density, and that drift volume and distance increase with wind speed and flight height. As a result, LiDAR-based drift-reduction metrics (e.g., DPR) can be directly used to evaluate nozzle drift-reduction classes and the potential for reducing buffer zone width [93]. However, this advantage relies on the prerequisite that spray clouds possess sufficient particle density and optical thickness. In scenarios with AIN or large-droplet, low-density sprays, LiDAR return signals weaken markedly or may even be absent, leading to systematic underestimation of drift risk. Conversely, in fine-spray, high-density conditions, LiDAR provides the most accurate response for cloud boundaries and maximum height [74]. Therefore, LiDAR is more adept at describing geometric structure than true mass distribution and may be effectively "blind" to long-range drift of a small number of high-momentum large droplets. LiDAR primarily captures geometric/plume structure proxies rather than true mass dis-tribution; therefore, it requires calibration/verification with deposition sampling. Under the typical UASS operating condition of "coarse droplets + near-ground downwash," relying solely on LiDAR signals will underestimate the penetration hazard of large droplets beyond the target zone.

To address this issue, some studies have proposed a "two-layer verification chain" combining LiDAR and deposition sampling. LiDAR is used to record the time-varying three-dimensional structure of plumes, while deposition samplers (e.g., WSP, PVC cards, PTFE lines) quantify deposition fluxes at different heights and downwind distances [26]. Using empirical models or machine learning methods, plume characteristic height, peak intensity, and horizontal spread can be mapped to deposition curves and buffer zone widths. This shift illustrates that the focus of field visualization is moving from "measurement accuracy per se" toward "how visualization-derived variables can be incorporated into standardized indicator systems and risk models."

For canopy "blind zones" that are difficult to observe directly behind the target, X-ray imaging provides a novel visualization perspective. Owing to its high penetrability, X-ray imaging can directly measure spray mass flux behind fruit trees or grape trellises and apply the Beer–Lambert law to invert attenuation into transmitted mass, thereby enabling quantitative characterization of canopy penetration rate, post-canopy drift risk, and mass drift [89,90]. Its unique value lies in revealing, from a mass-conservation standpoint, the spatial redistribution patterns of spray liquid that is partially blocked by the canopy yet still penetrates through it. However, due to its high cost and safety constraints, X-ray imaging

is better suited as a high-precision calibration tool in controlled environments than as a routine technique for large-scale field trials.

In real field conditions with composite flow, UASS must navigate non-stationary, three-dimensional flow fields created by rotor downwash and crosswind. Field visualization and deposition measurements consistently reveal that the angle between crosswind and downwash, wind speed fluctuations, and the relative position of nozzles within the rotor coverage all influence droplet transport pathways and drift sensitivity. When nozzles are located within the core of the rotor downwash, the downwash partially suppresses crosswind-induced uplift of fine droplets, concentrating drift within the 0–2 m near-ground layer. However, when nozzles move away from the downwash core or when crosswinds are stronger, fine droplets are more easily uplifted by the coupled crosswind-wake system, causing non-negligible drift at greater distances. These patterns have been verified using LiDAR plume trajectories, deposition patterns, and ground sampling [94]. Despite these insights, a unified parameterized drift representation across different UASS platforms, nozzle configurations, and environmental flow conditions remains absent, limiting the broader application of predictive models and operational guidelines. Field visualization research still exhibits three key gaps. First, most studies rely on a single sensor and lack multimodal coordination among LiDAR, laser imaging, thermal imaging, and deposition sampling, which hinders the construction of a complete causal chain from "flow-field disturbance" to "plume dispersion" to "target deposition." Second, although field drift standards like ISO 22866 [95] provide an experimental framework, there is no consensus on how to map LiDAR-derived plume variables or X-ray-based mass flux to these standardized drift indices. Third, existing studies mostly focus on open fields and simple orchards, with a notable lack of visual evidence for complex, three-dimensional environments such as large-canopy trees, multilayer canopies, or sloped terrain.

Thus, field visualization is not merely an extension of laboratory mechanism studies but serves as a critical link for validating the "wind tunnel–controlled environment–field" chain: it answers whether these flow–spray mechanisms still apply in real agricultural settings. Future UASS field research must focus on quantitatively transforming relationships between LiDAR/X-ray measurements and standardized deposition indices, building cross-platform, cross-scenario multimodal validation systems, and incorporating rotor–canopy vortex characteristics into drift metrics and buffer-zone decision models. This will propel field visualization from phenomenological observation toward predictive modeling and operational standardization.

4.3. Visualization and Equivalent Analysis of Rotor–Canopy Vortex Structures

In UASS, the interaction between rotor downwash and crop canopy constitutes the key dynamic mechanism governing droplet penetration, redistribution, and deposition patterns. Unlike conventional boom spraying, which primarily relies on jet momentum, the UASS flow field exhibits a dynamically evolving three-dimensional turbulent structure driven by blade periodicity, aircraft motion, and canopy resistance [44]. Therefore, some studies have argued that, particularly for deposition-oriented modeling, the objective of spray-flow visualization does not necessarily lie in full flow-field reconstruction, but rather in the identification of representative "vortical units" that exhibit stability, measurability, and parameterization potential, and can thus serve as dynamical proxy variables for deposition modeling [96].

A large body of PIV-, thermal-imaging-, and anemometer-array-based visualization evidence indicates that when rotor downwash impinges on the canopy top, the combined effects of canopy drag and wall attachment generate conical or toroidal vortex structures with well-defined boundaries, which exhibit strong temporal stability and can substantially

enhance spray penetration into the canopy interior. In wind tunnel experiments on a quadrotor UAV sprayer under controlled wind speed and liquid pressure conditions, deposition under Obvious Vortex (OV) regimes has been reported to be several times higher (up to 5–7×) than under non-vortical flow conditions, highlighting the potential contribution of vortical structures to spray utilization efficiency [85]. Similar stable structural features have also been confirmed in single-rotor tip-vortex studies. HSI and PIV results show that the tip-vortex core shifts systematically along the rotor radius, its core velocity decays logarithmically with increasing vortex age, and the structure transitions from laminar to turbulent [44]. More importantly, its dimensionless velocity distribution exhibits strong self-similarity, indicating that rotor vortices possess robust parameterization potential and can be used in spray dynamics modeling without requiring full CFD reconstruction.

Building on this, recent research has increasingly shifted from pursuing "complete flow-field reconstruction" to developing equivalent-flow representation methods based on vortical proxy variables. These approaches focus on indices such as vortex-core position, vortex area, vorticity intensity, and velocity gradients at the upper and lower boundaries of the vortex core. Compared with the full three-dimensional velocity field, these parameters are easier to acquire, more operationally practical, and exhibit higher explanatory power for deposition patterns. In joint rotor-disturbance–deposition experiments conducted by the authors' team in litchi canopies, deposition hotspots were found to be located at or near the vortex core. When canopy porosity or branch morphology caused the vortex to shift or weaken, the deposition pattern became "eccentric," with hotspot locations shifting in the same direction as the vortex-core displacement. This indicates that vortex position and morphology reveal deposition differences more effectively than traditional input variables, such as mean wind speed or turbulence intensity, and that they represent key dynamical mechanisms that conventional flow-field descriptors fail to capture [22].

Integrated visualization evidence from wind tunnels and field studies further indicates that, when vortex structures remain stable, deposition hotspot regions exhibit strong spatial consistency. In contrast, crosswind disturbances, canopy heterogeneity, or changes in rotor attitude rapidly alter vortex position, scale, and intensity, leading to deposition patterns that respond almost synchronously [23,85]. This strong coupling relationship forms the physical basis for constructing spray prediction models centered on vortex structures: deposition patterns are governed not only by the mean flow field but, to a greater extent, by "vortical dynamical units."

It should be emphasized that the vortex-centered perspective discussed above represents a conditional and modeling-oriented framework rather than a universal dominance assumption, and its applicability depends strongly on UASS configuration, canopy structure, and ambient flow conditions. Despite these advances, current vortex-related research still has three major limitations. First, many studies remain at the phenomenological level, describing the presence or absence of vortices, and lack systematic parameterization across UASS configurations (e.g., X4, X8, twin-rotor), canopy structures (canopy width, porosity), and flow-field conditions. How rotor layout, disk loading, canopy indices, and ambient turbulence jointly determine vortex intensity and stability remains ununified in a general explanatory framework. Second, mappings between vortex proxy variables and deposition behavior are mostly derived from case-specific scenarios and lack universal droplet–flow coupling criteria. For example, it remains unclear under which conditions vortices dominate deposition patterns and under which conditions crosswind dominates drift behavior—knowledge that is crucial for establishing vortex-based operational limit systems. Third, current vortex identification methods rely heavily on PIV or multi-point anemometer arrays, which are expensive and difficult to deploy rapidly in field settings [27]. Some studies have attempted to infer vortex-core locations from "density voids" in LiDAR

point clouds or "temperature depressions" in infrared thermal images, but whether these surrogate signals correspond to true vorticity peaks remains to be rigorously validated.

In summary, visualization studies of rotor–canopy vortices are constructing a structured, parameterizable dynamical framework for UASS spray deposition mechanisms: vortex structures are not merely by-products of the mean flow field but are dominant dynamical units for spray deposition, whose position, strength, and stability offer greater explanatory power than mean wind speed. Future research needs to advance in three key directions: (1) develop vortex parameterization models that span different UASS configurations and canopy environments, making vortex features standardized inputs for spray models; (2) create low-cost vortex identification methods that can be rapidly deployed in the field and directly support operational parameter decisions; and (3) explicitly embed vortex characteristics into deposition and drift prediction models, thereby achieving a transition from "phenomenological description" to "predictive modeling".

4.4. Model Integration and Application Expansion: From Visual Understanding to Computable Rules

The rapid development of visualization technologies has, for the first time, enabled multiscale observation of UASS spray processes from the nozzle near field through the rotor flow field and plume dispersion to target deposition. However, if this information remains confined to images, optical signals, or point clouds, its value will remain limited. Current research trends are shifting from "being able to see" to "being able to compute," that is, systematically embedding visualization results into spray dynamics and risk assessment models to construct structured, model-based predictive frameworks. This shift is reflected in three core aspects: reconstruction of near-field parameterized boundary conditions, model representation of mid- to far-field plume features, and learning-based predictive models built on multimodal visualization data.

At the near-field scale, visualization techniques have reshaped how nozzle atomization initial conditions are modeled. Traditional atomization and drift models often rely on fixed $Dv_{0.5}$, typical initial velocities, and nominal spray angles. In contrast, combined applications of PDPA, PDIA, HSI, and DIH have demonstrated a pronounced coupling between droplet size distribution and initial velocity, jointly influenced by pressure, nozzle geometry, and liquid physical properties. Representative studies have derived empirical relationships via regression analysis in which droplet velocity increases with the square root of pressure and decreases with increasing median diameter, with coefficients of determination exceeding 0.9 [34]. Empirical formulations distilled from such visualization results enable CFD and semi-empirical drift models to use realistic "joint distributions of droplet size and velocity" as boundary conditions, rather than relying on prior assumptions, thereby significantly improving the fidelity of UASS spray initial-momentum representations. Meanwhile, visualization has also revealed dynamic variations in spray angle during operation, showing that nozzle mounting orientation, incoming-flow shear, and boom vibration all affect the "effective spray angle" and thereby introduce systematic shifts in plume spatial distribution. This information provides necessary corrections to model input structures, making near-field visualization the starting point for building credible modeling chains.

At the mid- to far-field scale, visualization techniques such as LiDAR, laser imaging, and laser light-sheet scanning enable quantification of key plume variables—such as geometric structure, spread width, centroid trajectory, and return intensity—thereby providing new structural inputs for drift prediction models. Traditional drift models rely on meteorological and operational parameters such as wind speed, spray rate, and flight height to construct one-dimensional empirical formulations. Visualization-based methods provide more process-representative structural variables, including plume characteristic

height, plume center position, plume width, cloud centroid trajectory, and drift indices derived from grayscale or return signals (e.g., DIX, DPR). These variables extend drift prediction from "one-dimensional distance estimation" to "structured plume modeling," in which plume geometry and transport structure are explicitly included, enabling models to reflect the dynamic influence of flow-field changes on spray dispersion. In other words, visualization not only supplies validation data but also determines which key control variables can be defined and quantified within the model.

In addition, the multimodal nature of visualization is driving fusion modeling to become a dominant trend. Droplet and velocity fields (PDPA/DIH), rotor-vortex features (PIV/thermal imaging), plume point clouds (LiDAR), and deposition patterns (WSP, PVC, X-ray) essentially form "data slices" of the UASS spray system at different scales. If each subsystem is modeled in isolation, it is difficult to uncover the critical causal chain by which "rotor-flow disturbances, mediated through vortex structures, influence droplet transport and ultimately determine canopy deposition responses." Consequently, some studies have begun to construct unified variable systems that integrate droplet statistics ($Dv_{0.1}$, $Dv_{0.5}$, $Dv_{0.9}$, RSF), velocity statistics (mean velocity, velocity fluctuations), flow-field indicators (vorticity, vortex-core strength, effective downwash velocity), plume morphology parameters (characteristic height, centroid trajectory), and deposition responses (inter-layer deposition gradients, ground settling, airborne drift) into a multidimensional parameter space, and then apply multivariate regression, PLS, or machine learning models to identify key control variables [97]. In this process, visualization's role shifts from a "data provider" to a determinant of which intermediate variables can be defined, thereby restructuring the explanatory framework of spray dynamics. However, multimodal fusion modeling also introduces substantial methodological challenges. High collinearity among visualization-derived features may obscure true control mechanisms and inflate apparent model performance if not properly addressed. Moreover, correlation-driven learning frameworks alone are insufficient to disentangle causal relationships between flow structures, droplet transport, and deposition outcomes, particularly under the limited sample sizes typical of UASS experiments. Without explicit feature selection, regularization, cross-scenario validation, and physics-informed constraints, multimodal models are prone to overfitting and poor generalization, and their interpretability remains limited. Addressing these issues is essential for transforming multimodal fusion from a descriptive integration concept into a reliable modeling strategy.

Despite rapid progress in multimodal fusion models, structural limitations remain. First, many models are still confined to "within-scenario interpolation," that is, local fitting around existing experimental conditions, with insufficient cross-validation across UASS platforms, crops, and meteorological conditions. As a result, such models are difficult to apply directly to engineering standards or regulatory frameworks. Second, novel visualization variables, such as vortex strength and plume geometry, lack unified units or definitions, hindering cross-platform comparisons and model transfer. Third, most existing models adopt a "static concatenation" feature structure, directly merging outputs from different sensors into a feature vector without fully exploiting the temporal and causal structure of spray processes, and thus cannot comprehensively capture the chain of "rotor-parameter change–flow-field reconfiguration–droplet transport–deposition response".

Therefore, future breakthroughs in UASS spray modeling will not come from simply incorporating more visualization devices but from building cross-platform, cross-scenario reusable parameter systems centered on a small set of equivalent dynamical variables with clear physical meaning—such as vortex strength, effective downwash velocity, driftable volume fraction, and characteristic plume height—and explicitly embedding them into

spray dynamics models and intelligent decision frameworks. Only by achieving a closed loop of "observable–quantifiable–computable" can visualization truly drive UASS spraying from experiment-dependent to prediction-driven operation.

5. Intelligent Processing and Analysis of Visualization Data

With the development of machine learning and deep learning, UASS spray research is rapidly shifting from "physical observation" toward a pipeline of "computable features–predictive modeling–parameter decision-making." Large volumes of visualization data (e.g., HSI, DIH point clouds, LiDAR plumes, PIV time-resolved flow fields) are being transformed into structured variables suitable for modeling, supporting nozzle characterization, flow-field identification, drift prediction, and spray parameter optimization. Privitera et al. [53] noted that droplet-spectrum prediction models based on CNNs, ANNs, and regression algorithms exhibit high stability across multiple factors, including nozzle type, spray pressure, and adjuvant concentration, thereby providing strong support for the construction of an integrated "sensing–modeling–prediction" spray monitoring framework. However, current intelligent analysis still has clear limitations: on the one hand, most models rely on single-modality data and thus struggle to generalize across different nozzles, environments, and platforms; on the other hand, feature extraction and variable definitions vary across research groups, making cross-platform modeling and result alignment challenging. It is therefore necessary, at the methodological level, to systematically integrate image-level recognition, multimodal feature extraction, and predictive modeling.

Beyond enhancing predictive accuracy, intelligent processing of visualization data is increasingly expected to support decision-making from both economic and environmental perspectives. Studies have shown that optimized flow rates, nozzle–flight parameter combinations, and drift-aware control strategies can reduce pesticide use, minimize off-target losses, and mitigate environmental risks, thereby enhancing the overall cost-effectiveness of UASS operations [43,47]. However, these benefits are typically assessed indirectly through deposition efficiency or drift-reduction metrics rather than explicit economic evaluations.

5.1. Image-Level Recognition of Droplet and Flow-Field Features

Image-level recognition is the entry point through which visualization data enter computational models, and its quality directly determines the upper bound of subsequent modeling. Early spray image analysis relied mainly on traditional algorithms, such as threshold segmentation, edge detection, and Hough transforms [17]. Under simple background conditions, these methods can accomplish droplet size statistics [98], but their errors increase sharply in high-concentration, strongly scattering, and heavily overlapping spray fields [81], and manual parameter tuning is labor-intensive.

With the introduction of deep learning, the automation and robustness of droplet recognition have improved significantly. CNN-based detection frameworks (such as YOLO and Mask R-CNN) have been applied to PDIA, HSI, and DIH images [55], and can maintain high accuracy under polydisperse droplet spectra, complex illumination, or local defocus conditions [99]. Network-architecture optimizations for small-object detection and enhanced feature pyramids enable improved YOLO variants to achieve mAP values above 0.9 for droplet detection, and, when combined with multi-object tracking algorithms (e.g., DeepSORT), to perform droplet tracking and counting across image sequences. It should be noted that such performance metrics are typically obtained under controlled droplet densities and moderate optical depths, and may degrade in high-density sprays with severe droplet overlap or strong multiple-scattering effects. The GSConv-enhanced YOLOv5s + DeepSORT framework proposed by Chen et al. [100] achieves real-time detec-

tion at about 100 fps, with counting errors of about 6%, indicating that droplet detection is transitioning from offline statistics to real-time quality assessment.

For flow-field visualization, AI methods have been employed to automatically identify structural features such as vortices, recirculation zones, and primary downwash streams from PIV vector fields and smoke-flow images. In rotor–canopy coupled flow fields, ConvLSTM, U-Net, and optical-flow networks have been used to reconstruct velocity fields or automatically segment vortical regions [55]. Paired with a classification scheme of Obvious Vortex (OV), Slight Vortex (SV), and No Vortex (NV), these approaches generate disturbance labels with physical meaning, facilitating the establishment of correspondences between disturbance levels and deposition patterns [22,101].

It is important to emphasize that the key aspect of image recognition is not merely "detection accuracy," but whether the results reflect the true underlying physical processes. For example, in near-nozzle regions, PDPA tends to underestimate the volume fraction of large droplets due to its spherical-drop assumption, whereas PDIA or HSI can more realistically capture droplet-spectrum structure [77]. Therefore, explicitly incorporating quality-control indicators such as defocus degree and sphericity into deep learning models helps build physics-informed detection frameworks, avoiding the "learning" of instrument biases and enhancing the credibility of measurements and the interpretability of the resulting models.

5.2. Multimodal Feature Fusion and Associative Modeling

A major advantage of UASS spray visualization lies in its ability to simultaneously acquire multi-source data on droplet spectra, flow fields, plumes, and target deposition. Constructing a multimodal fusion framework is thus a critical step in moving from "visualized phenomena" to "computable regularities." However, different instruments (PDPA, LD, DIH, PIV, LiDAR) differ systematically in measurement principles, droplet-size limits, and error structures [74,76,102]. Directly fusing their outputs without methodological alignment can undermine model credibility [53,77].

To mitigate this problem, research has begun to promote fusion across three levels: data, features, and models. At the data level, fusion typically uses geometric calibration and temporal synchronization to map outputs from different sensors into a unified coordinate system, enabling the comparison of droplet spectra, flow fields, and deposition-board measurements within the same physical space. At the feature level, PCA, PLS, or embedded-space methods are used to compress high-dimensional descriptors—such as liquid-film hole angle, breakup morphology, vortex indicators, and plume width—into low-dimensional, interpretable variables. For example, Cryer and Li et al. [39,103] extracted 14 geometric features of liquid-film breakup and used principal component regression to predict D10, D50, and D90, demonstrating the potential of image geometric features as proxy variables for droplet spectra.

At the model level, droplet-spectrum parameters (Dv_{50}, RSF), aerodynamic features (downwash velocity, vortex strength, downwash–crosswind angle), spatial-structure metrics (plume center, three-dimensional point-cloud density), and canopy porosity are jointly fed into ANNs, GWO-ANNs, or multimodal fusion networks to predict deposition uniformity and airborne drift [21,85,101]. Existing studies have reported that incorporating flow-field or vortex-related features can improve the apparent explanatory capability of deposition models, suggesting a physical complementarity between droplet intrinsic parameters and aerodynamic-structure descriptors [46]. However, these improvements are typically evaluated within individual studies, and quantitative benchmarks or independent cross-scenario validations remain limited, which constrains direct comparison across different modeling frameworks.

To facilitate the construction of reusable feature systems across platforms and UASS types, droplet-field characteristics reported in current research can be abstracted into four categories: droplet intrinsic properties, aerodynamic properties, spatial structure, and temporal dynamics. Table 5 summarizes 14 core features across three categories and their typical acquisition methods, providing a crucial foundation for constructing unified embedding spaces and multimodal associative models.

Table 5. Multimodal droplet field characteristics system and typical acquisition methods.

Type	Characteristic Quantity	Meaning and Function	Typical Measurement Methods	Representative References (Examples)
Droplet properties	Dv_{10}	Droplet size corresponding to 10% volume fraction, used to describe fine droplets, sensitive to drift risk.	Laser diffraction, PDPA, HSI/DIH	De Cock et al., 2016; Tuck et al., 1997 [66,104]
	Dv_{50} (VMD)	Median diameter of volume distribution, core indicator of droplet coarseness.	LD, PDPA, imaging/DIH	Tuck et al., 1997 [104]
	Dv_{90}	Droplet size corresponding to 90% volume fraction, used to describe coarse droplets, sensitive to deposition ability.	LD, PDPA, DIH	De Cock et al., 2016 [66]
	RSF (Relative Span)	$(Dv_{90}–Dv_{10})/Dv_{50}$, describes droplet spectrum width, related to droplet polydispersity and deposition distribution uniformity.	LD, PDPA, image analysis	Tuck et al., 1997 [104]
	D_{32} (Sauter Mean Diameter)	Equivalent diameter linking volume and surface area, represents mass transfer/evaporation and deposition processes.	PDPA, DIH, image analysis	Kumar et al., 2024 [55]
	Droplet Number Density/Volume Fraction	Number or volume fraction of droplets per unit volume, basis for constructing mass flux and risk assessment.	DIH, HSI, X-ray, LiDAR/laser imaging	Kumar et al., 2024; Heindel, 2018 [55,89]
	Droplet Morphology/Breakage Mode	Liquid film, filaments, agglomerated droplets, related to nozzle internal flow patterns and breakage mechanisms.	HSI, image pattern recognition	Kumar et al., 2024 [101]
Aerodynamics	Downwash Velocity Field (u, w)	Rotor-induced 3D velocity field, determines droplet initial acceleration and down/upward trends.	PIV, hot-wire/Doppler, CFD + experimental inversion	Liu et al., 2021 [85]
	Vortex Strength/Vorticity	The strength and scale of wingtip vortices, directly affecting droplet entrainment and upward drift.	PIV, CFD, rotor wind tunnel experiments	Wang et al., 2021 [21]
	Vortex Core Location and Trajectory	The spatial path of vortex cores, determining the position and height of secondary upward drift.	PIV, CFD configuration, laser imaging comparison	Liu et al., 2021 [85]
	Downwash–Crosswind Angle	The resultant flow direction after combining external wind field and rotor downwash, influencing drift main direction and plume deflection.	Wind tunnel tests, on-site meteorological measurements + UASS posture recording	Delpuech et al., 2022; Liu et al., 2021 [51,85]
Spatial structure	Plume Width	The lateral expansion scale of the droplet cloud, key parameter for safety buffer zone and spray width coverage.	LiDAR, laser slicing imaging, DIH 3D field	Gil et al., 2013; Wang et al., 2024 [54,74]
	Plume Centroid Position	The position of the droplet cloud's center in horizontal and vertical directions, representing overall drift tendency and lift.	LiDAR point cloud reconstruction, laser imaging, 3D DIH	Gil et al., 2013; Wang et al., 2023 [74,75]
	Three-dimensional Droplet Density Field/Voxel Occupancy	The distribution of droplets in 3D space and local enrichment areas, basis for constructing 3D drift models and canopy penetration analysis.	LiDAR 3D scanning, DIH, laser plane scanning	Wang et al., 2024; Kumar et al., 2024; Wang et al., 2023 [54,55,75]

5.3. Intelligent Prediction and Spray Parameter Optimization

After completing image-level recognition and feature fusion, the ultimate goal is to transform these structured variables into predictive models that can support spraying decisions, including drift distance, deposition uniformity, and optimized combinations of nozzle and flight parameters [34,35,53]. Existing research mainly progresses along two pathways: (1) constructing empirical and machine-learning models based on LiDAR,

laser imaging, and droplet-spectrum parameters [54,55]; and (2) directly building end-to-end prediction frameworks from image or time-series data [39,105].

In drift modeling, multiple linear regression, SVR, random forests, and DNNs have been used to fit relationships between variables such as characteristic plume height, wind speed, and Dv_{50} and corresponding drift responses, underscoring the importance of structural visualization parameters in drift modeling [34,38,53]. For control and optimization, Kumar et al. [101] employed GWO-ANN to automatically search network structures and hyperparameters and used flight height, speed, and flow rate to predict deposition metrics, demonstrating the advantages of swarm-intelligence optimization and ANNs in spray tuning. In addition, a more interpretable line of work attempts to construct droplet-spectrum prediction models directly from high-speed spray videos. Li et al. [103] used an LDA topic model to extract "atomization topics" from image sequences and regressed them against D_{50}, enabling high-accuracy discrimination of different spray conditions. Such "image pattern–physical parameter" mappings exhibit clear advantages in low-sample scenarios.

For drift inversion, LiDAR plume point clouds have been used to infer ground deposition distributions, with some studies establishing mappings between plume centroid trajectories and deposition curves, thereby offering potential alternatives to portions of standardized drift test benches [54]. It must be noted, however, that LiDAR is insensitive to droplet size and to low-density fields dominated by large droplets; accordingly, model construction must explicitly account for these measurement biases rather than treating LiDAR returns as direct proxies for true concentration [53,77].

Overall, intelligent prediction and parameter optimization based on visualization data still face three main bottlenecks. First, models are often trained on a single platform or scenario, which limits their generalization. Second, many models lack explicit physical constraints, limiting their extrapolation capability. Third, due to the absence of real-time acquisition of flow-field and plume features, closed-loop control practices remain insufficient [28,39]. These limitations are particularly critical because, in practical spraying operations, intelligent optimization is ultimately expected to reduce unnecessary spray losses, improve deposition efficiency, and mitigate operational and environmental costs. However, most existing studies evaluate these benefits indirectly through deposition and drift metrics, and comprehensive cost–benefit analyses that explicitly integrate visualization-derived indicators remain scarce. Achieving a genuine "sense–predict–act" real-time loop in the future will therefore require further advances in multi-modal data acquisition, physics-informed learning, and edge deployment.

6. Conclusions and Prospects

UASS couple nozzle atomization, rotor-induced flow fields, ambient airflows, and crop canopy structure into a typical multiscale two-phase flow system, making it difficult to directly extrapolate from traditional boom-sprayer spray mechanisms and drift concepts. Centered on the core chain of "droplets–flow field–target," this paper provides a systematic review of the physical foundations of spray atomization and transport, visualization monitoring technologies, wind tunnel and field validation platforms, and intelligent analysis and modeling methods based on visualization data, thereby offering a structured cognitive framework for UASS spraying.

At the mechanistic level, nozzles determine the initial droplet-size and velocity distributions, while rotor downwash and ambient winds jointly shape the complex transport pathway of "depression–entrainment–uplift–redeposition." Hydraulic nozzles produce broad droplet spectra and are highly sensitive to perturbations, whereas centrifugal nozzles yield more concentrated and adjustable droplet-size distributions. Local vortex structures generated by rotor–canopy coupling have been shown to be closely associated with pene-

tration and deposition hotspots, forming the key dynamical units that distinguish UASS from traditional boom spraying.

At the visualization-monitoring level, HSI, PDIA, DIH, laser diffraction, and PDPA constitute fine-scale characterization tools for nozzle near fields; LiDAR, laser light-sheet scanning, and X-ray imaging enable three-dimensional reconstruction of mid- to far-field plumes; and PIV and wind tunnel/controlled-environment platforms reveal coupling mechanisms among rotor flow fields, canopy disturbances, and droplet motion. Although a multi-platform cross-validation framework involving wind tunnels, field trials, and numerical simulations is gradually emerging, inconsistencies in measurement principles, statistical methods, and reported parameters remain major bottlenecks that hinder model transfer across platforms.

At the application and intelligent-analysis level, visualization data have progressively evolved from "phenomenological display" to quantitative support for nozzle selection, operational parameter optimization, and risk assessment. Wind tunnel platforms provide controlled boundaries for calibrating nozzles, adjuvants, and CFD/AgDRIFT models; field LiDAR and related tools verify the actual effects of spray height, spray volume, and buffer-zone design; and deep learning has enhanced automated identification of droplet spectra, vortex structures, and plumes. However, most existing intelligent models remain confined to single platforms, small datasets, and offline prediction; feature systems lack unification; and measurement biases are difficult to reconcile across studies, so that a true closed loop of "sensing–prediction–control" has yet to be realized.

Building on the above systematic analysis, future research on UASS spray visualization and modeling can focus on the following three directions:

(1) Multiscale model cross-validation and standardization based on a unified feature system

In line with the preceding discussion, future work on UASS spray visualization and intelligent modeling should first make breakthroughs in feature-system standardization and multiscale cross-validation. At present, droplet-spectrum, flow-field, and drift data exhibit high heterogeneity in terms of nozzle types, measurement methods, and platform conditions, making it difficult to establish strict comparability across studies. Based on ISO standards and recent advances in cross-technology comparisons, there is an urgent need to define a set of core features that can be shared across platforms and to develop unified schemes for feature extraction, reporting, and cross-validation across nozzle test benches, wind tunnels, and field trials. Establishing multiscale information mappings from near-field atomization to far-field deposition via intermediate variables—such as logistic-function parameters, vortex-strength indices, and LiDAR point-cloud features—will be a foundational task for future model construction and validation.

(2) Wind–spray–target coupled modeling oriented toward vortex–canopy interactions

An increasing body of evidence indicates that the interaction between rotor-induced vortices and canopy porosity is the key dynamical mechanism governing droplet penetration, deposition hotspots, and re-entrainment behavior. Future research needs to shift from traditional empirical relationships between "mean wind speed and mean deposition" to a coupling framework centered on "vortex structure–canopy disturbance–deposition pattern." By using PIV, HSI, DIH, and LiDAR to extract parameterizable vortex indices—including vortex-core position, scale, and strength—and combining these with canopy porosity and deposition requirements at sensitive target locations, it will be possible to develop structured, interpretable, and generalizable wind–spray–target coupling models. Such models can provide theoretical support for nozzle layout, flight-strategy design, and precise on-target spraying under complex conditions (e.g., sloping terrain, headwind operations, and large-canopy fruit trees).

(3) Intelligent closed-loop control driven by embedded multimodal sensing

The ultimate goal of droplet visualization is not merely process characterization, but its evolution toward intelligent closed-loop control driven by embedded sensing. With ongoing advances in sensor miniaturization and edge-computing capabilities, onboard vision systems, lightweight LiDAR/DIH, and deep-learning inference will progressively enable real-time droplet-spectrum identification, spray-width monitoring, and drift-plume tracking on UASS. Combined with physics-constrained online prediction models, this will support adaptive adjustment of spray rate, droplet size (e.g., centrifugal nozzle rotation speed), flight height, and velocity, thereby establishing a closed-loop system for coordinated regulation of "environment–flow field–operational parameters." On this basis, building open visualization databases and spray knowledge graphs will help establish UASS operational regulations, risk classification schemes, and certification systems, thereby enabling a transition from "visualization-based monitoring" to "intelligent operational decision-making".

Overall, UASS spray visualization research is undergoing a transformation from "two-dimensional droplet spectra" to "multidimensional droplet fields," and from "experimental characterization" to "intelligent decision support." As long as steady progress is made in the three key areas of feature standardization, vortex–canopy coupling modeling, and embedded closed-loop control, future UASS are expected to achieve a true leap from "being observable" to "being accurately computable and controllable," thereby providing a more solid scientific and technological foundation for efficient, safe, and environmentally friendly agricultural aerial spraying.

Author Contributions: Conceptualization, Z.C. and X.L.; methodology, H.Z. and P.W.; software, P.C. and X.L.; validation, M.T. and Z.C.; formal analysis, P.W. and M.T.; investigation, M.T. and P.W.; resources, J.M. and H.Z.; data curation, P.W. and X.L.; writing—original draft preparation, P.C., Z.C. and X.L.; writing—review and editing, J.M., Z.C. and P.C.; visualization, H.Z. and M.T.; supervision, J.M. and Z.C.; project administration, J.M. and P.C.; funding acquisition, H.Z. and P.C. All authors have read and agreed to the published version of the manuscript.

Funding: This research was supported by the Xinjiang Talent Development Fund's Second Round of 2025 Funding—Special Program for Talent Team Support of Scientific Research and Innovation Platforms, and the Guangdong Province Basic and Applied Basic Research Fund (2023A1515110564).

Data Availability Statement: No new data were created or analyzed in this study. Data sharing is not applicable to this article.

Acknowledgments: We would like to acknowledge the support from the Xinjiang Agricultural Unmanned Aerial Vehicle Performance and Safety Key Laboratory for providing technical assistance. During the preparation of this manuscript, the authors used the Gemini 3.0 AI model for the purpose of assisting in the conceptualization of one schematic figure. The authors have reviewed and edited the output and take full responsibility for the content of this publication.

Conflicts of Interest: The authors declare no conflicts of interest.

References

1. Anken, T.; Coupy, G.; Dubuis, P.H.; Favre, G.; Geiser, H.C.; Gurba, A.; Häni, M.; Hochstrasser, M.; Landis, M.; Maitre, T. Plant protection treatments in Switzerland using unmanned aerial vehicles: Regulatory framework and lessons learned. *Pest Manag. Sci.* **2025**, *81*, 3419–3429. [CrossRef]
2. Wang, L.; Huang, X.; Li, W.; Yan, K.; Han, Y.; Zhang, Y.; Pawlowski, L.; Lan, Y. Progress in agricultural unmanned aerial vehicles (UAVs) applied in China and prospects for Poland. *Agriculture* **2022**, *12*, 397. [CrossRef]
3. Freeman, P.K.; Freeland, R.S. Politics & technology: US polices restricting unmanned aerial systems in agriculture. *Food Policy* **2014**, *49*, 302–311. [CrossRef]

4. Ivezić, A.; Trudić, B.; Stamenković, Z.; Kuzmanović, B.; Perić, S.; Ivošević, B.; Buđen, M.; Petrović, K. Drone-related agrotechnologies for precise plant protection in western balkans: Applications, possibilities, and legal framework limitations. *Agronomy* **2023**, *13*, 2615. [CrossRef]
5. Nahiyoon, S.A.; Ren, Z.; Wei, P.; Li, X.; Li, X.; Xu, J.; Yan, X.; Yuan, H. Recent development trends in plant protection UAVs: A journey from conventional practices to cutting-edge technologies—A comprehensive review. *Drones* **2024**, *8*, 457. [CrossRef]
6. Zhan, Y. Optimization of Rotor Layout and Energy Consumption Test of Multi-Wing Single-Arm Structure Electric UAV. Master's Thesis, South China Agricultural University, Guangzhou, China, 2019.
7. Tahir, M.N.; Lan, Y.; Zhang, Y.; Wenjiang, H.; Wang, Y.; Naqvi, S.M.Z.A. Application of unmanned aerial vehicles in precision agriculture. In *Precision Agriculture*; Elsevier: Amsterdam, The Netherlands, 2023; pp. 55–70.
8. Bian, Z. Research on Vector Anti-Drift System for Plant Protection Unmanned Aerial Vehicle. Master's Thesis, Shandong University of Technology, Zibo, China, 2024.
9. Lan, Y. *Precision Agricultural Aviation Application Technology*; Springer Nature: Berlin/Heidelberg, Germany, 2025; ISBN 3031899172.
10. Lv, M.; Xiao, S.; Yu, T.; He, Y. Influence of UAV flight speed on droplet deposition characteristics with the application of infrared thermal imaging. *Int. J. Agric. Biol. Eng.* **2019**, *12*, 10–17. [CrossRef]
11. Fritz, B.K.; Hoffmann, W.C.; Bagley, W.E.; Kruger, G.R.; Czaczyk, Z.; Henry, R.S. Measuring droplet size of agricultural spray nozzles− measurement distance and airspeed effects. *At. Spray* **2014**, *24*, 747–760. [CrossRef]
12. Xu, Y.; Han, Y.; Sun, Z.; Gu, W.; Jin, Y.; Xue, X.; Lan, Y. Path planning optimization with multiple pesticide and power loading bases using several unmanned aerial systems on segmented agricultural fields. *IEEE Trans. Syst. Man Cybern. Syst.* **2022**, *53*, 1882–1894. [CrossRef]
13. *ISO 16122-5:2020*; Agricultural and Forestry Machines—Inspection of Sprayers in use—Part 5: Aerial Spray Systems. International Organization for Standardization (ISO): Geneva, Switzerland, 2020.
14. *ISO 5682-1:2017*; Equipment for Crop Protection—Spraying Equipment—Part 1: Test Methods for Sprayer Nozzles. International Organization for Standardization (ISO): Geneva, Switzerland, 2017.
15. *ISO 24253-1:2015*; Crop Protection Equipment—Spray Deposition Test for Field Crop—Part 1: Measurement in a Horizontal Plane. International Organization for Standardization (ISO): Geneva, Switzerland, 2015.
16. Saleem, S.R.; Zaman, Q.U.; Schumann, A.W.; Naqvi, S.M.Z.A. Variable rate technologies: Development, adaptation, and opportunities in agriculture. In *Precision Agriculture*; Elsevier: Amsterdam, The Netherlands, 2023; pp. 103–122.
17. Kashdan, J.T.; Shrimpton, J.S.; Whybrew, A. A digital image analysis technique for quantitative characterisation of high-speed sprays. *Opt. Laser Eng.* **2007**, *45*, 106–115. [CrossRef]
18. Gavali, P.; Kalashetty, S. Experimental Analysis of Droplet Characterisation of Centrifugal-Assisted Sprayer. *J. Inst. Eng. (India) Ser. C* **2023**, *104*, 1023–1030. [CrossRef]
19. Zheng, Y.; Yang, S.; Yubin, L.; Hoffmann, C.; Chunjiang, Z.; Liping, C.; Xingxing, L.; Yu, T. A novel detection method of spray droplet distribution based on LIDARs. *Int. J. Agric. Biol. Eng.* **2017**, *10*, 54–65. [CrossRef]
20. Luo, S.; Wen, S.; Zhang, L.; Lan, Y.; Chen, X. Extraction of crop canopy features and decision-making for variable spraying based on unmanned aerial vehicle LiDAR data. *Comput. Electron. Agric.* **2024**, *224*, 109197. [CrossRef]
21. Wang, L.; Xu, M.; Hou, Q.; Wang, Z.; Lan, Y.; Wang, S. Numerical verification on influence of multi-feature parameters to the downwash airflow field and operation effect of a six-rotor agricultural UAV in flight. *Comput. Electron. Agric.* **2021**, *190*, 106425. [CrossRef]
22. Lan, Y.; Liu, H.; Chen, P.; Ma, G.; Wu, J.; Liao, J.; Ma, H.; Qiu, J.; Qin, Y. Time series model for predicting the disturbance of lychee canopy by wind field in unmanned aerial spraying system. *Comput. Electron. Agric.* **2025**, *231*, 109954. [CrossRef]
23. Chang, K.; Chen, S.; Wang, M.; Xue, X.; Lan, Y. Numerical simulation and verification of rotor downwash flow field of plant protection UAV at different rotor speeds. *Front. Plant Sci.* **2023**, *13*, 1087636. [CrossRef]
24. Zhang, R.; Chen, L.; Wen, Y.; Tang, Q.; Li, L. Key technologies for testing and analyzing aerial spray deposition and drift: A comprehensive review. *Int. J. Precis. Agric. Aviat.* **2020**, *3*, 13–27. [CrossRef]
25. Chegini, G.; Ashtiani-Araghi, A.; Tekin, A.B.; Lee, C. Laboratory Methods for the Measurement of Spray Characteristics of the Nozzles in UAV Sprayers: A Review. *J. Biosyst. Eng.* **2025**, *50*, 1–20. [CrossRef]
26. Molnar-irimie, A.; Ranta, O.; STĂNILĂ, S.; Marian, O. Study Regarding Methods and Techniques Used for Analysis of Spray Drift and Droplet Size Distribution by Agricultural Spraying Machines. *Bull. Univ. Agric. Sci. Vet. Med. Cluj-Napoca. Agric.* **2025**, *82*, 1–11. [CrossRef]
27. Zhan, Y.; Chen, P.; Xu, W.; Chen, S.; Han, Y.; Lan, Y.; Wang, G. Influence of the downwash airflow distribution characteristics of a plant protection UAV on spray deposit distribution. *Biosyst. Eng.* **2022**, *216*, 32–45. [CrossRef]
28. Makhnenko, I.; Alonzi, E.R.; Fredericks, S.A.; Colby, C.M.; Dutcher, C.S. A review of liquid sheet breakup: Perspectives from agricultural sprays. *J. Aerosol Sci.* **2021**, *157*, 105805. [CrossRef]
29. Jackiw, I.M.; Ashgriz, N. On aerodynamic droplet breakup. *J. Fluid Mech.* **2021**, *913*, A33. [CrossRef]

30. Wang, G.; Zhang, T.; Song, C.; Yu, X.; Shan, C.; Gu, H.; Lan, Y. Evaluation of spray drift of plant protection drone nozzles based on wind tunnel test. *Agriculture* **2023**, *13*, 628. [CrossRef]
31. Tadić, V.; Radočaj, D.; Jurišić, M. Machine Learning Methods for Evaluation of Technical Factors of Spraying in Permanent Plantations. *Agronomy* **2024**, *14*, 1977. [CrossRef]
32. Cerruto, E.; Manetto, G.; Papa, R.; Longo, D. Modelling spray pressure effects on droplet size distribution from agricultural nozzles. *Appl. Sci.* **2021**, *11*, 9283. [CrossRef]
33. Nogueira Martins, R.; Freitas, M.A.M.D.; Lima, A.D.C.; Furtado Junior, M.R. Effect of nozzle type and pressure on spray droplet characteristics. *Idesia* **2021**, *39*, 101–107. [CrossRef]
34. Dorr, G.J.; Hewitt, A.J.; Adkins, S.W.; Hanan, J.; Zhang, H.; Noller, B. A comparison of initial spray characteristics produced by agricultural nozzles. *Crop Prot.* **2013**, *53*, 109–117. [CrossRef]
35. Yu, S.; Kim, Y.; Jun, H.; Choi, I.S.; Woo, J.; Kim, Y.; Yun, Y.; Choi, Y.; Alidoost, R.; Lee, J. Evaluation of Spray Characteristics of Pesticide Injection System in Agricultural Drones. *J. Biosyst. Eng.* **2020**, *45*, 272–280. [CrossRef]
36. Prado, E.P.; Guerreiro, J.C.; Ferreira-Filho, P.J.; Do Nascimento, V.; Ferrari, S.; Galindo, F.S.; Funichello, M.; Raetano, C.G.; Pagliari, P.H.; Chechetto, R.G. Performance of spray nozzles and droplet size on glufosinate deposition and weed biological efficacy. *Crop Prot.* **2024**, *177*, 106560. [CrossRef]
37. Canu, R.; Puggelli, S.; Essadki, M.; Duret, B.; Menard, T.; Massot, M.; Reveillon, J.; Demoulin, F.X. Where does the droplet size distribution come from? *Int. J. Multiph. Flow* **2018**, *107*, 230–245. [CrossRef]
38. Alidoost Dafsari, R.; Yu, S.; Choi, Y.; Lee, J. Effect of geometrical parameters of air-induction nozzles on droplet characteristics and behaviour. *Biosyst. Eng.* **2021**, *209*, 14–29. [CrossRef]
39. Cryer, S.; Raymond, J. Interpreting Image Patterns for Agricultural Sprays Using Statistics and Machine Learning Techniques. *Fluids* **2024**, *9*, 40. [CrossRef]
40. *ISO 25358:2018*; Crop Protection Equipment—Droplet-Size Spectra from Atomizers—Measurement and Classification. International Organization for Standardization: Geneva, Switzerland, 2018.
41. Calderone, G.; Catania, P.; Comparetti, A.; Ferro, M.V.; Greco, C.; Vallone, M.; Orlando, S. Spray deposition efficiency of unmanned aerial spraying systems in hillside vineyards with variable slope. *Smart Agric. Technol.* **2025**, *12*, 101386. [CrossRef]
42. Chen, P.; Douzals, J.P.; Lan, Y.; Cotteux, E.; Delpuech, X.; Pouxviel, G.; Zhan, Y. Characteristics of unmanned aerial spraying systems and related spray drift: A review. *Front. Plant Sci.* **2022**, *13*, 870956. [CrossRef]
43. Wang, S.; Dorr, G.J.; Khashehchi, M.; He, X. Performance of selected agricultural spray nozzles using particle image velocimetry. *J. Agric. Sci. Tech.* **2015**, *17*, 601–613.
44. Ansaripour, M.; Dafsari, R.A.; Yu, S.; Choi, Y.; Lee, J. Characteristics of a tip-vortex generated by a single rotor used in agricultural spraying drone. *Exp. Therm. Fluid Sci.* **2023**, *149*, 110995. [CrossRef]
45. Guo, S.; Li, J.; Yao, W.; Zhan, Y.; Li, Y.; Shi, Y. Distribution characteristics on droplet deposition of wind field vortex formed by multi-rotor UAV. *PLoS ONE* **2019**, *14*, e220024. [CrossRef] [PubMed]
46. Coombes, M.; Newton, S.; Knowles, J.; Garmory, A. The influence of rotor downwash on spray distribution under a quadrotor unmanned aerial system. *Comput. Electron. Agric.* **2022**, *196*, 106807. [CrossRef]
47. Hewitt, A.J. Spray drift: Impact of requirements to protect the environment. *Crop Prot.* **2000**, *19*, 623–627. [CrossRef]
48. Fritz, B.K.; Hoffmann, W.C. Measuring Spray Droplet Size from Agricultural Nozzles Using Laser Diffraction. *J. Vis. Exp.* **2016**, *115*, 54533. [CrossRef]
49. Hu, S.; Xu, X.; Liu, J.; Guo, J.; Guan, R.; Zhou, Z.; Lan, Y.; Chen, S. Movement Characteristics of Droplet Deposition in Flat Spray Nozzle for Agricultural UAVs. *Agriculture* **2024**, *14*, 1994. [CrossRef]
50. Wang, C.; Herbst, A.; Zeng, A.; Wongsuk, S.; Qiao, B.; Qi, P.; Bonds, J.; Overbeck, V.; Yang, Y.; Gao, W.; et al. Assessment of spray deposition, drift and mass balance from unmanned aerial vehicle sprayer using an artificial vineyard. *Sci. Total Environ.* **2021**, *777*, 146181. [CrossRef]
51. Delpuech, X.; Pouxviel, G.; Cotteux, E.; Verges, A.; Douzals, J. Evaluation of aerial drift during drone spraying of an artificial vineyard. *Ives Tech. Rev. Vine Wine* **2022**. [CrossRef]
52. Wen, S.; Han, J.; Ning, Z.; Lan, Y.; Yin, X.; Zhang, J.; Ge, Y. Numerical analysis and validation of spray distributions disturbed by quad-rotor drone wake at different flight speeds. *Comput. Electron. Agric.* **2019**, *166*, 105036. [CrossRef]
53. Privitera, S.; Manetto, G.; Pascuzzi, S.; Pessina, D.; Cerruto, E. Drop Size Measurement Techniques for Agricultural Sprays:A State-of-The-Art Review. *Agronomy* **2023**, *13*, 678. [CrossRef]
54. Wang, Z.; Qi, P.; Li, Y.; He, X. Visualization of Aerial Droplet Distribution for Unmanned Aerial Spray Systems Based on Laser Imaging. *Drones* **2024**, *8*, 613. [CrossRef]
55. Kumar, M.S.; Hogan, C.J.; Fredericks, S.A.; Hong, J. Visualization and characterization of agricultural sprays using machine learning based digital inline holography. *Comput. Electron. Agric.* **2024**, *216*, 108486. [CrossRef]
56. Bachalo, W.D. Method for measuring the size and velocity of spheres by dual-beam light-scatter interferometry. *Appl. Opt.* **1980**, *19*, 363–370. [CrossRef] [PubMed]

57. Nuyttens, D.; De Schampheleire, M.; Steurbaut, W.; Baetens, K.; Verboven, P.; Nicolai, B.; Ramon, H.; Sonck, B. Characterization of agricultural sprays using laser techniques. *Asp. Appl. Biol.* **2006**, *77*, 179.
58. Lodwik, D.; Pietrzyk, J.; Malesa, W. Analysis of volume distribution and evaluation of the spraying spectrum in terms of spraying quality. *Appl. Sci.* **2020**, *10*, 2395. [CrossRef]
59. Albrecht, H.; Damaschke, N.; Borys, M.; Tropea, C. *Laser Doppler and Phase Doppler Measurement Techniques*; Springer Science & Business Media: Berlin/Heidelberg, Germany, 2013; ISBN 3662051656.
60. Melling, A. Tracer particles and seeding for particle image velocimetry. *Meas. Sci. Technol.* **1997**, *8*, 1406. [CrossRef]
61. Tropea, C. Optical particle characterization in flows. *Annu. Rev. Fluid Mech.* **2011**, *43*, 399–426. [CrossRef]
62. Fansler, T.D.; Parrish, S.E. Spray measurement technology: A review. *Meas. Sci. Technol.* **2014**, *26*, 12002. [CrossRef]
63. Coghe, A.; Cossali, G.E. Quantitative optical techniques for dense sprays investigation: A survey. *Opt. Laser Eng.* **2012**, *50*, 46–56. [CrossRef]
64. Adrian, R.J.; Westerweel, J. *Particle Image Velocimetry*; Cambridge University Press: Cambridge, UK, 2011.
65. Raffel, M.; Willert, C.E.; Scarano, F.; Kähler, C.J.; Wereley, S.T.; Kompenhans, J. *Particle Image Velocimetry: A Practical Guide*; Springer: Berlin/Heidelberg, Germany, 2018.
66. De Cock, N.; Massinon, M.; Nuyttens, D.; Dekeyser, D.; Lebeau, F. Measurements of reference ISO nozzles by high-speed imaging. *Crop Prot.* **2016**, *89*, 105–115. [CrossRef]
67. Wang, L.; Zhang, L.; Lin, W.; Wu, Y.; Wu, X. Spray trajectory and 3D droplets distribution of liquid jet in crossflow with digital inline holography. *Exp. Therm. Fluid Sci.* **2022**, *139*, 110725. [CrossRef]
68. Wu, Y.; Wang, L.; Lin, W.; Song, G.; He, Y.; Wu, X.; Wang, Z.; Cen, K. Picosecond pulsed digital off-axis holography for near-nozzle droplet size and 3D distribution measurement of a swirl kerosene spray. *Fuel* **2021**, *283*, 119124. [CrossRef]
69. Trolinger, J.D.; Mansoor, M.M. History and metrology applications of a game-changing technology: Digital holography. *J. Opt. Soc. Am. A* **2022**, *39*, A29–A43. [CrossRef]
70. Pan, G.; Meng, H. Digital holography of particle fields: Reconstruction by use of complex amplitude. *Appl. Optics* **2003**, *42*, 827–833. [CrossRef] [PubMed]
71. Carreira, V.D.S.; Nuyttens, D.; Langenakens, J.; Pereira, J.V.; Da Silva, R.P. Smartphone image-based framework for quick, non-invasive measurement of spray characteristics. *Smart Agric. Technol.* **2023**, *3*, 100120. [CrossRef]
72. Acharya, P.; Burgers, T.; Nguyen, K. AI-enabled droplet detection and tracking for agricultural spraying systems. *Comput. Electron. Agric.* **2022**, *202*, 107325. [CrossRef]
73. Stiti, M.; Garcia, S.; Lempereur, C.; Doublet, P.; Kristensson, E.; Berrocal, E. Droplet sizing in atomizing sprays using polarization ratio with structured laser illumination planar imaging. *Opt. Lett.* **2023**, *48*, 4065–4068. [CrossRef]
74. Gil, E.; Llorens, J.; Llop, J.; Fàbregas, X.; Gallart, M. Use of a Terrestrial LIDAR Sensor for Drift Detection in Vineyard Spraying. *Sensors* **2013**, *13*, 516–534. [CrossRef] [PubMed]
75. Wang, Z.; Zhang, Y.; Li, T.; Müller, J.; He, X. Visualization of Lidar-Based 3D Droplet Distribution Detection for Air-Assisted Spraying. *Agriengineering* **2023**, *5*, 1136–1146. [CrossRef]
76. Privitera, S.; Cerruto, E.; Manetto, G.; Lupica, S.; Nuyttens, D.; Dekeyser, D.; Zwertvaegher, I.; Furtado Júnior, M.R.; Vargas, B.C. Comparison between Liquid Immersion, Laser Diffraction, PDPA, and Shadowgraphy in Assessing Droplet Size from Agricultural Nozzles. *Agriculture* **2024**, *14*, 1191. [CrossRef]
77. Sijs, R.; Kooij, S.; Holterman, H.J.; van de Zande, J.; Bonn, D. Drop size measurement techniques for sprays: Comparison of image analysis, phase Doppler particle analysis, and laser diffraction. *AIP Adv.* **2021**, *11*, 15315. [CrossRef]
78. Li, L.; Zhang, R.; Chen, L.; Hewitt, A.J.; He, X.; Ding, C.; Tang, Q.; Liu, B. Toward a remote sensing method based on commercial LiDAR sensors for the measurement of spray drift and potential drift reduction. *Sci. Total Environ.* **2024**, *918*, 170819. [CrossRef]
79. Ramasamy, M.; Johnson, B.; Leishman, J.G. Turbulent tip vortex measurements using dual-plane stereoscopic particle image velocimetry. *AIAA J.* **2009**, *47*, 1826–1840. [CrossRef]
80. Zhang, H.; Qi, L.; Wan, J.; Musiu, E.M.; Zhou, J.; Lu, Z.; Wang, P. Numerical simulation of downwash airflow distribution inside tree canopies of an apple orchard from a multirotor unmanned aerial vehicle (UAV) sprayer. *Comput. Electron. Agric.* **2022**, *195*, 106817. [CrossRef]
81. Murphy, S.D.; Mortimer, V.; Lydon, M. Droplet sizing and imaging of agricultural sprays using particle/droplet image analysis. In Proceedings of the International Conference on Pesticide Application for Drift Management, Waikoloa, HI, USA, 27–29 October 2004; WSU: Pullman, WA, USA, 2004; pp. 324–329.
82. *ISO 22856: 2008*; Equipment for Crop Protection—Methods for the Laboratory Measurement of Spray Drift—Wind Tunnels. International Organization for Standardization (ISO): Geneva, Switzerland, 2008.
83. *GB/T 32241-2015*; Standardization Administration of China: Methods for Testing Spray Drift of Pesticide Application. China Standards Press: Beijing, China, 2015.
84. Wang, Z.; He, X.; Li, T.; Huang, M.; Zhang, Y.; Xu, L.; Deng, X.J. Evaluation method of pesticide droplet drift based on laser imaging. *Trans. Csae* **2019**, *35*, 73–79.

85. Liu, Q.; Chen, S.; Wang, G.; Lan, Y. Drift Evaluation of a Quadrotor Unmanned Aerial Vehicle (UAV) Sprayer: Effect of Liquid Pressure and Wind Speed on Drift Potential Based on Wind Tunnel Test. *Appl. Sci.* **2021**, *11*, 7258. [CrossRef]
86. Cui, Z.; Cui, L.; Yan, X.; Han, Y.; Yang, W.; Zhan, Y.; Wu, J.; Qin, Y.; Chen, P.; Lan, Y. Field Evaluation of Different Unmanned Aerial Spraying Systems Applied to Control Panonychus citri in Mountainous Citrus Orchards. *Agriculture* **2025**, *15*, 1283. [CrossRef]
87. Shi, X.; Du, Y.; Liu, X.; Liu, C.; Hou, Q.; Chen, L.; Yong, R.; Ma, J.; Yang, D.; Yuan, H. Optimizing UAV spray parameters to improve precise control of tobacco pests at different growth stages. *Pest Manag. Sci.* **2024**, *80*, 5809–5819. [CrossRef]
88. Wang, G.; Lan, Y.; Qi, H.; Chen, P.; Hewitt, A.; Han, Y. Field evaluation of an unmanned aerial vehicle (UAV) sprayer: Effect of spray volume on deposition and the control of pests and disease in wheat. *Pest Manag. Sci.* **2019**, *75*, 1546–1555. [CrossRef]
89. Heindel, T.J. X-ray imaging techniques to quantify spray characteristics in the near field. *At. Spray* **2018**, *28*, 1029–1059. [CrossRef]
90. Qiu, S.; Wang, S.; Zhang, Y.; Li, X.; Hung, D.; Xu, M. Dense-field spray droplet size quantification of flashing boiling atomization using structured laser illumination planar imaging technique. *Fuel* **2023**, *335*, 127085. [CrossRef]
91. Zhang, H.; Wen, S.; Chen, C.; Liu, Q.; Xu, T.; Chen, S.; Lan, Y. Downwash airflow field distribution characteristics and their effect on the spray field distribution of the DJI T30 six-rotor plant protection UAV. *Int. J. Agric. Biol. Eng.* **2023**, *16*, 10–22. [CrossRef]
92. Liu, Q.; Shan, C.; Zhang, H.; Song, C.; Lan, Y. Evaluation of liquid atomization and spray drift reduction of hydraulic nozzles with four spray adjuvant solutions. *Agriculture* **2023**, *13*, 236. [CrossRef]
93. Torrent, X.; Gregorio, E.; Rosell-Polo, J.R.; Arnó, J.; Peris, M.; van de Zande, J.C.; Planas, S. Determination of spray drift and buffer zones in 3D crops using the ISO standard and new LiDAR methodologies. *Sci. Total Environ.* **2020**, *714*, 136666. [CrossRef]
94. Kasbi, M.K.; Dafsari, R.A.; Charanandeh, A.; Yu, S.; Choi, Y.; Lee, J. Parametric study on the internal geometry affecting agricultural air induction nozzle performance. *Phys. Fluids* **2023**, *35*, 023316. [CrossRef]
95. *ISO 22866:2005*; Equipment for crop protection—Methods for Field Measurement of Spray Drift. International Organization for Standardization (ISO): Geneva, Switzerland, 2008.
96. Tang, Q.; Zhang, R.; Chen, L.; Deng, W.; Xu, M.; Xu, G.; Li, L.; Hewitt, A. Numerical simulation of the downwash flow field and droplet movement from an unmanned helicopter for crop spraying. *Comput. Electron. Agric.* **2020**, *174*, 105468. [CrossRef]
97. Mazzi, G.; Becce, L.; Ali, A.; Bortolini, M.; Gregoris, E.; Feltracco, M.; Barbaro, E.; Gronauer, A.; Gambaro, A.; Mazzetto, F. Methodological Advancements in Testing Agricultural Nozzles and Handling of Drop Size Distribution Data. *Agriengineering* **2025**, *7*, 139. [CrossRef]
98. Minov, S.; Cointault, F.; Vangeyte, J.; Pieters, J.; Nuyttens, D. Spray Droplet Characterization from a Single Nozzle by High Speed Image Analysis Using an In-Focus Droplet Criterion. *Sensors* **2016**, *16*, 218. [CrossRef]
99. Huynh, N.; Nguyen, K. Real-Time Droplet Detection for Agricultural Spraying Systems: A Deep Learning Approach. *Mach. Learn. Knowl. Extr.* **2024**, *6*, 259–282. [CrossRef]
100. Chen, S.; Liu, J.; Xu, X.; Jianzhou, G.; Shiyun, H.; Zhiyan, Z.; Yubin, L. Detection and tracking of agricultural spray droplets using GSConv-enhanced YOLOv5s and DeepSORT. *Comput. Electron. Agric.* **2025**, *235*, 110353. [CrossRef]
101. Kumar, S.P.; Jat, D.; Sahni, R.K.; Jyoti, B.; Kumar, M.; Subeesh, A.; Parmar, B.S.; Mehta, C.R. Measurement of droplets characteristics of UAV based spraying system using imaging techniques and prediction by GWO-ANN model. *Measurement* **2024**, *234*, 114759. [CrossRef]
102. Gil, E.; Gallart, M.; Balsari, P.; Marucco, P.; Almajano, M.P.; Llop, J. Influence of wind velocity and wind direction on measurements of spray drift potential of boom sprayers using drift test bench. *Agric. For. Meteorol.* **2015**, *202*, 94–101. [CrossRef]
103. Li, H.; Cryer, S.; Acharya, L.; Raymond, J. Video and image classification using atomisation spray image patterns and deep learning. *Biosyst. Eng.* **2020**, *200*, 13–22. [CrossRef]
104. Tuck, C.R.; Ellis, M.B.; Miller, P. Techniques for measurement of droplet size and velocity distributions in agricultural sprays. *Crop Prot.* **1997**, *16*, 619–628. [CrossRef]
105. Li, H.; Cryer, S.; Raymond, J.; Acharya, L. Interpreting atomization of agricultural spray image patterns using latent Dirichlet allocation techniques. *Artif. Intell. Agric.* **2020**, *4*, 253–261. [CrossRef]

Disclaimer/Publisher's Note: The statements, opinions and data contained in all publications are solely those of the individual author(s) and contributor(s) and not of MDPI and/or the editor(s). MDPI and/or the editor(s) disclaim responsibility for any injury to people or property resulting from any ideas, methods, instructions or products referred to in the content.